Journal of Atmospheric and Solar–Terrestrial Physics 210 (2020) 105437

Contents lists available at ScienceDirect

Journal of Atmospheric and Solar-Terrestrial Physics

journal homepage: www.elsevier.com/locate/jastp

Research Paper

Artificial neural network application in an implemented lightning locating system

Kamyar Mehranzamir [a,*], Zulkurnain Abdul-Malek [b], Hadi Nabipour Afrouzi [c], Saeed Vahabi Mashak [b], Chin-leong Wooi [d], Roozbeh Zarei [e]

[a] Department of Electrical and Electronic Engineering, Faculty of Science and Engineering, University of Nottingham Malaysia, Jalan Broga, 43500, Semenyih, Selangor, Malaysia
[b] Institute of High Voltage and High Current, School of Electrical Engineering, Faculty of Engineering, Universiti Teknologi Malaysia, Johor Bahru, Malaysia
[c] Faculty of Engineering, Computing & Science, Swinburne University of Technology Sarawak, Malaysia
[d] Centre of Excellence for Renewable Energy, Faculty of Electrical Engineering Technology, Universiti Malaysia Perlis Pauh Putra Campus, 02600 Arau, Perlis, Malaysia
[e] School of Information Technology, Deakin University, Melbourne, Australia

ARTICLE INFO

Keywords:
Lightning detection
Artificial neural network (ANN)
Time difference of arrival (TDOA)
Lightning discharge

ABSTRACT

Time difference of arrival (TDOA) technique is one of many bases to determine lightning strike location employed in a lightning locating system (LLS). In this technique, at least four measurement sensors are required to correctly locate a lightning strike. Usage of fewer number of sensors will result in non-unique solutions to the generated hyperbolas, and hence wrong lightning strike point. This research aims to correctly determine the strike point even if only three measuring sensors are utilized. An artificial neural network (ANN) based algorithm was developed for a 400 km^2 coverage area in Southern Malaysia using time of arrival data collected at the three measuring stations over a certain period. The Levenberg–Marquardt algorithm is demonstrated to correctly identify the lightning strike coordinates with an average error of 350 m. The algorithm has helped the three-station TDOA-based LLS to successfully locate the lightning strike point with a remarkable accuracy comparable to that of commercial systems.

1. Introduction

Lightning discharges are manifestation of processes that generate, separate and lastly neutralize electrical charges in nature through thunderstorms. Lightning is associated with many different atmospheric and surface processes including severe weather conditions (Siingh et al., 2015). Lightning strike is a great concern to mankind because of its detrimental impact on human safety, hazard and equipment failures. Throughout the world, many lives are lost every year due to lightning related incidents. In fact, lightning related fatalities and damages are higher in countries with higher rates of thunderstorm days, such as in Malaysia.

There are several types of lightning discharges. These are categorized as the cloud to cloud (CC) or inter-cloud discharge, the intra-cloud (IC) discharge, the cloud to air discharge, and the cloud to ground (CG) discharge. A lightning discharge emits significant electromagnetic radiation with broadband frequencies from a few hertz in the very low frequency (VLF) band to several hundreds MHz (approximately 300 MHz), or the very high frequency (VHF) band. The actual measured values of the peak magnitude and the frequency spectrum depends on the distance from which the lightning electromagnetic field is measured. In addition, electromagnetic radiation with frequencies over 300 MHz up to 300 GHz, or the extra high frequency (EHF) band is also reported (Rakov, 2016; Sun et al., 2013).

A CG lightning starts with an initial electric breakdown in the cloud followed by leader channels. A series of branching channels grow within a cloud to form a branch channel structure. A CG strike may cause harm and damages to ground objects during the discharge process. Studies had previously been carried out to better understand the discharge behaviour and its consequent threats to man-made systems. Various instruments and structures including current measuring towers, antennas and high-speed cameras have been employed to characterize the discharges (Jiang et al., 2014; Wang et al., 2018). Optical observations were made by Jiang et al. (2020) and then the data were used to

* Corresponding author.
E-mail addresses: kamyar.mehranzamir@nottingham.edu.my (K. Mehranzamir), zulkurnain@utm.my (Z. Abdul-Malek), hafrouzi@swinburne.edu.my (H. Nabipour Afrouzi), vmsaeed3@live.utm.my (S. Vahabi Mashak), clwooi@unimap.edu.my (C.-l. Wooi), roozbeh.zarei@gmail.com (R. Zarei).

https://doi.org/10.1016/j.jastp.2020.105437
Received 22 March 2020; Received in revised form 17 August 2020; Accepted 18 August 2020
Available online 17 September 2020

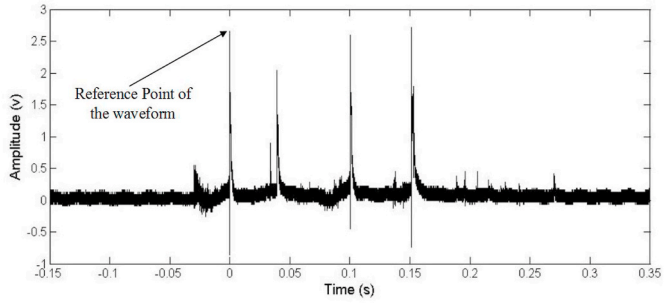

Fig. 1. Selection of the peak of first return stroke as the reference point of a lightning waveform.

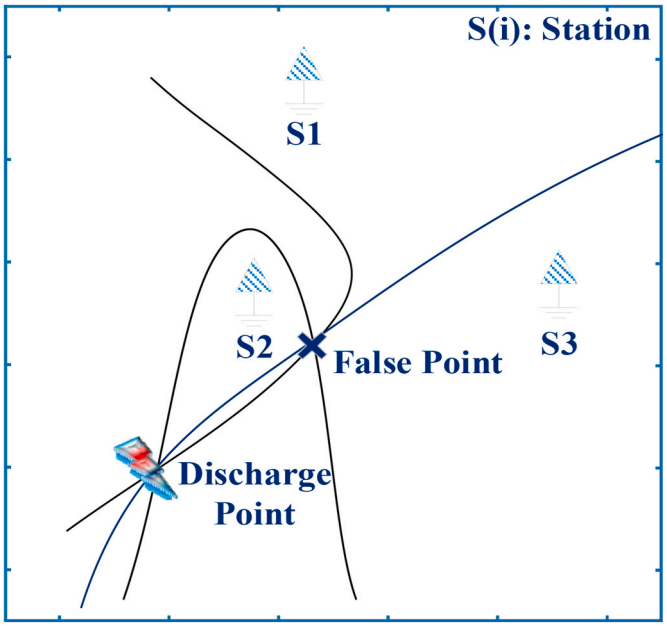

Fig. 2. Intersections of hyperbola-like lines or curves formed between each of two stations for locating lightning flashes using three sensors, leading to two solutions (true discharge and false discharge points).

simulate the CG lightning near tall structures. Their findings demonstrated that there is a direct relationship between the lightning protection system and the protected structure height. The effects of the atmospheric conditions as well as the existence of ground objects on lightning behaviour are also widely studied. For example, Yaniv et al. (2017) measured the atmospheric vertical electric fields at different measuring stations to find the correlation between the daily electric field and the time of the day. Studies have also been performed to determine the over the sea lightning discharge intensities. Asfur et al. (2020) hypothesized that the intensity of lightning depends on the concentration of salt, such that water with a higher electrical conductivity can conduct a higher peak current.

Most importantly, researches had shown that lightning is a major cause of power system breakdowns throughout the world (Singh et al., 2011), especially for regions with high lightning activities, such as Malaysia. It is known that the geographical location influences the surrounding atmosphere and hence the characteristics of a lightning discharge. Malaysia is situated near the Equator and has an average of 200 thunderstorm days per year. Therefore, the need for continuous improvement towards a more effective lightning protection system cannot be overemphasized. For example, to reduce the number of electric supply interruptions, lightning detection and protection systems have now incorporated the real time data which include the location of

Fig. 3. Locations of measurement stations, IVAT station (1.560447, 103.643542), B11 station (1.557839, 103.635694), and VAN station (1.565997, 103.633469).

lightning discharge, the classification of lightning type, and the provision of warning and alert to impending severe lightning activities (Kadir et al., 2012).

A country wide lightning locating system (LLS) currently available in Malaysia can facilitate such early warning of hazards to the public and hence allow them to apply protective and safety procedures. An LLS usually consists of several sensors located at different locations, and hence the name of multi-station LLS. However, for a small area application and with a lower detection accuracy, it can also be based on just a single-station. Of course, a multi-station LLS is more accurate and has a larger coverage, but its principal equipment and facilities are more expensive. An LLS can be achieved based on one or more main techniques or working principles. Three main working principles of an LLS are the time difference of arrival (TDOA), the interferometry, and the magnetic direction finding (MDF) (Bent et al., 1983; Maier et al., 1983; Orville, 1994). Many researchers have investigated the performance of these LLS techniques, including the combined techniques, such as the combination of TDOA and MDF sensors (Cummins et al., 1998; Koshak and Solakiewicz, 2001; Wood and Inan, 2003). Also, variations in each technique may be implemented for specific applications. Sun et al. (2013) performed a study on a short-baseline TDOA LLS using four identical antennas. To amend its accuracy, a parabolic interpolation algorithm was employed to improve the time resolution of the locating system. Their observations by high-speed cameras and captured electrical fields were combined to map the lightning radiation source in two dimensions.

The detection accuracy is an important aspect of an LLS, more so when the accuracy of a lightning location is critical in certain applications such as insurance claims. The TDOA technique is known to be one of the more accurate lightning detection methods (Underwood, 2006). In a TDOA-based LLS, a lightning discharge causes the generation and propagation of electromagnetic field which is then detected by the TDOA sensors, the arrival time at each sensor is dependent on the sensor location (Behnam Salimi et al., 2013). The difference of arrival times between any two stations is used to define a hyperbola equation. The intersection of these hyperbolas can be used to define the lightning striking point. However, in a three-station TDOA-based LLS, giving three hyperbola equations, a non-unique but rather two intersection points are produced. Hence, at least four antennas or stations are required to define a unique striking point.

In the TDOA technique, even a small uncertainty in the timestamps

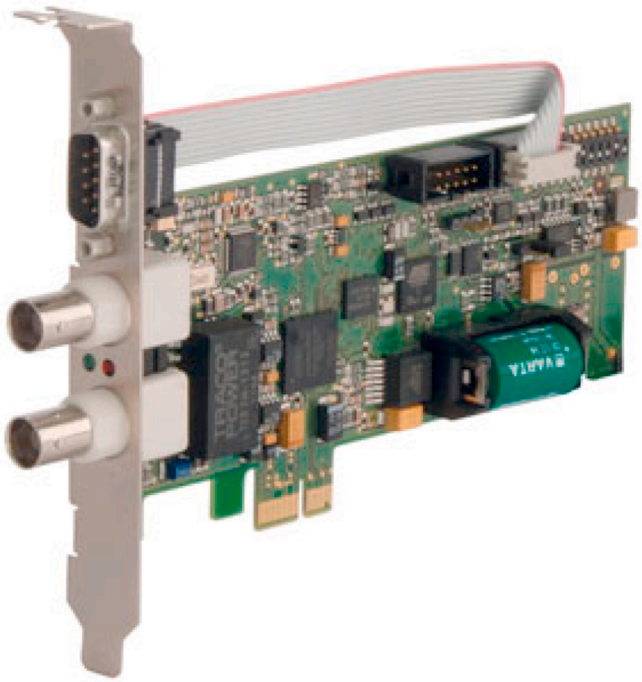

(a)

(b)

Fig. 4. GPS180PEX: (a) Low-profile global positioning system (GPS) clock (PCI Express), (b) GPS antenna installed on building roof.

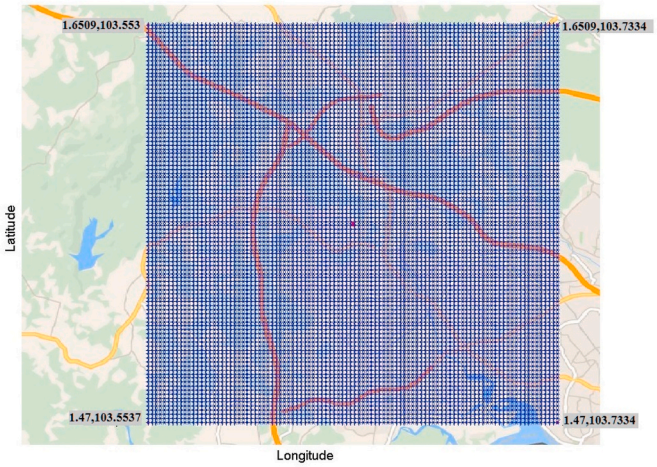

Fig. 5. Dividing the coverage area into 3600 points (blue points) as simulated lightning strike points (input points) for training artificial neural networks (ANNs).

may result in a rather large uncertainty in the computed location of the lightning strike. The detection accuracy of the system is dependent on the timing uncertainty, and is independent from the distances between the sensors and the lightning strike location. The timing accuracy can be improved using the global positioning system (GPS), which is a space-based satellite navigation system that provides location and time information in all weather conditions. In a typical LLS application, a GPS set includes GPS card and antenna. It is able to record the position (latitude, longitude) of the measuring stations, and more importantly, the timestamps of the captured lightning discharge. Very accurate GPS cards with nanosecond precision provide a synchronized LLS and record precise timestamps. It is to be noted that, in TDOA-based LLS, the measured electromagnetic fields are those associated with very-low-frequency and low-frequency radiation, both of which are usually associated with the cloud-to-ground discharges (Keogh et al., 2006).

As previously discussed, at least four sensors are needed for a TDOA-based LLS to give a unique lightning location. In this work, we demonstrate that it is possible to locate a lightning discharge even though only three sensors are used. In fact, the correct intersection point between the three obtained hyperbolas can be determined with the help of artificial intelligence. With the proposed usage of intelligence, the minimum number of sensor stations can be reduced from the previously four to three, and hence a saving in hardware costs. This research paper is divided into several sections. Section 1 provides the introduction, background, and literature review. Section 2 discusses the computational algorithm calculations for the three-station based TDOA method. Section 3 describes the coordinates of three installed stations and hardware installation in South Malaysia. Section 4 brings up the methodology of the current research, including the application of the artificial neural network (ANN). In Section 5, the structure and formation of the proposed ANN engines are described. The results of the trained ANNs are presented in Section 6. This section discusses the simulation and experimental results of the proposed flowcharts, as obtained from the simulations and practical experiments. The simulation results of the detection method are investigated in terms of the detection accuracy inside the coverage area. Finally, the conclusion of this research is given in Section 7.

2. Computational algorithm

A lightning flash generates a series of electromagnetic fields which propagate over the surface of the Earth. The location of a lightning strike can be estimated if several synchronized stations can capture the arrival time instants of a common strike. The time difference of arrival (TDOA)

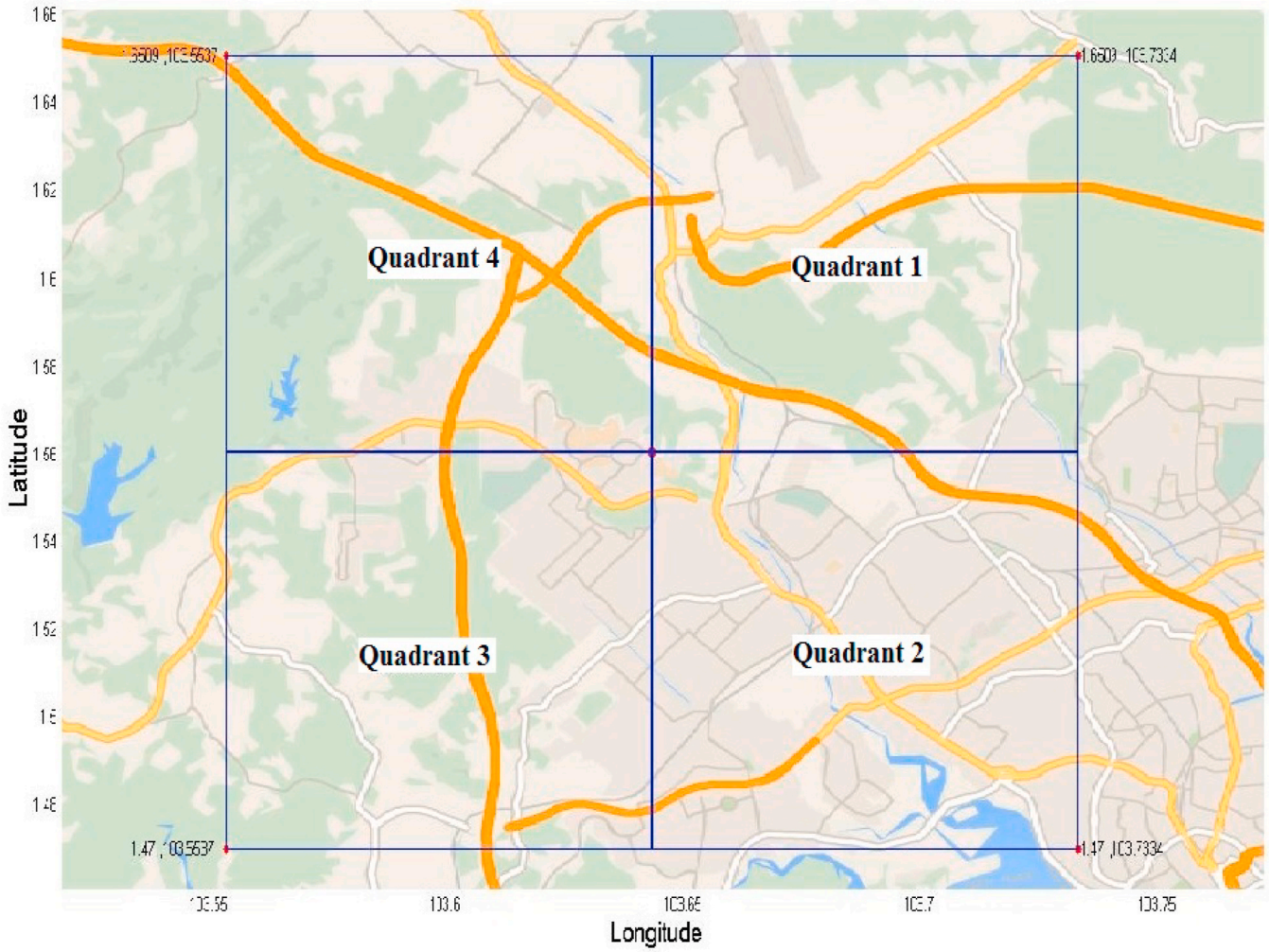

Fig. 6. Sectionalising coverage area in Fig. 5 into four quadrants with respect to IVAT station (1.560447, 103.643542).

method operates over a wide range of frequencies in most lightning location systems. For instance, this method has been applied in the low-frequency range for several lightning detection systems installed in the USA, Europe, and Asia. The very-low-frequency and low-frequency radiations of cloud-to-ground lightning discharges propagate mostly near 10 kHz frequency (Cummins et al., 2008; Cummins and Murphy, 2009; Gulyás et al., 2006). The name of the TDOA method hints at the method it depends on, as described in the following sentences. A timestamp is saved at each station by an accurate GPS antenna and card upon receiving a lightning signal. A sample of a selected reference point (peak point of the first return stroke) of a ground flash is presented in Fig. 1. The differences in the time of arrivals of the captured waveforms between stations are then determined. The time differences are used to form hyperbolas around the three stations. A unique intersection point of all hyperbolas gives the striking point of the lightning discharge.

The TDOA method utilises the timestamps detected by GPS antennas where each station receives the same discharge signal but at different time instants (Chen et al., 2015; Vahabi-Mashak et al., 2015). Precise GPS cards can supply more accurate times and hence more accurate locations for the TDOA method. A GPS card with nanosecond resolution provides a high-resolution time precision for the system. As previously described, a captured time difference between any two measuring stations forms a hyperbola. Fig. 2 illustrates that there are two intersection points from all three hyperbolas. Again, as previously noted, at least four stations are needed for determining a unique common intersection point of all hyperbolas (Chen et al., 2015; Cummins and Murphy, 2009). It is noted that the sensor stations should be at fixed locations with fixed coordinates. In some applications, mobile stations may be used. In this case, the actual operating mobile sensor coordinate can be easily set inside the computer program.

The TDOA approach relies on measuring the arrival times of lightning flashes at stations in different locations. The peak current of the first return stroke detected at different time instants at the stations are used to produce an ensemble of possible locations of a lightning strike hitting the ground. The position of antenna 1 (S1) is assigned to be the reference point, with a coordinate of (0,0). The coordinates of antenna 2 (S2) and antenna 3 (S3) are represented by (x_2, y_2) and (x_3, y_3), respectively. The radiation source is considered to happen at (x, y), which is also in Cartesian coordinates. The z coordinate value is considered 0 in all cases, that is all strikes are assumed to be cloud-to-ground strikes, and hence not considered in the derivation. The Pythagorean Theorem states that the sum of the squares of the lengths of the legs is equal to the square of the length of the hypotenuse (the side opposite the right angle). Therefore, the respective distances of antenna 1, antenna 2, and antenna 3 to the radiation source (r_1, r_2, and r_3) are determined as follows:

$$r_1 = \sqrt{x^2+y^2} \tag{1}$$

$$r_2 = \sqrt{(x-x_2)^2+(y-y_2)^2} \tag{2}$$

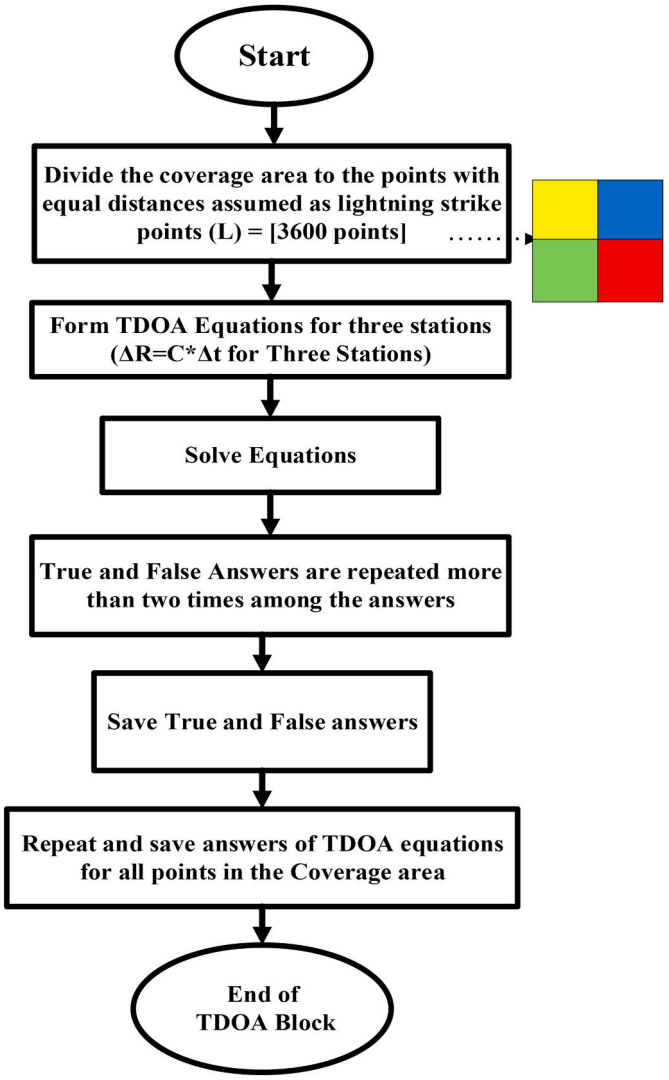

Fig. 7. Flowchart of TDOA calculations for all four quadrants in the coverage area for three stations.

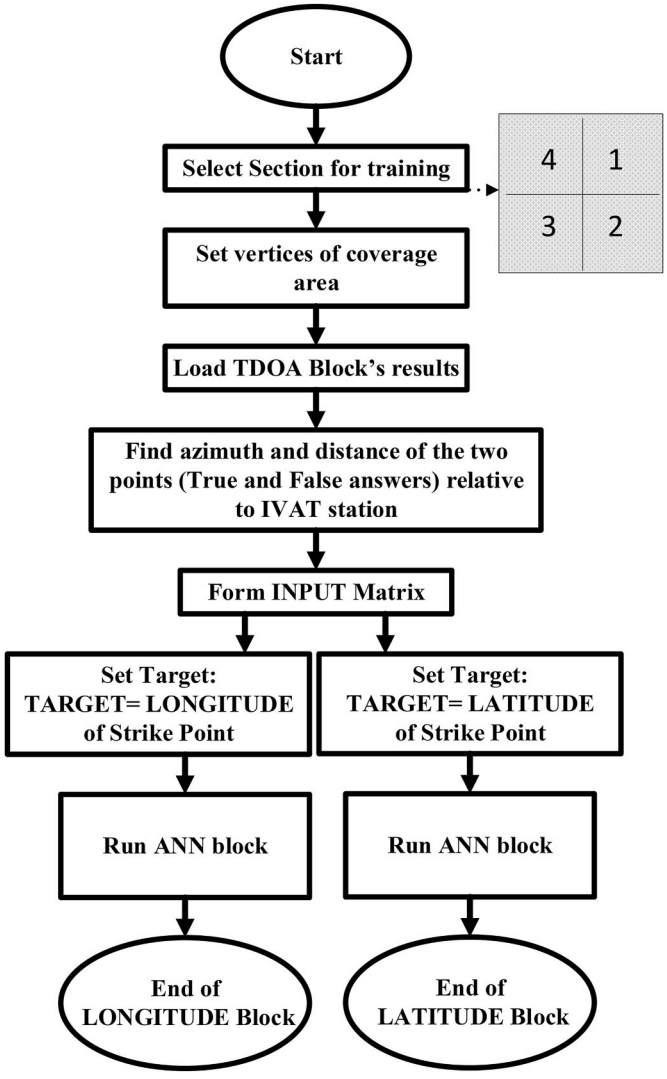

Fig. 8. Flowchart of using ANN for finding longitude and latitude of strike point in quadrants 1 to 4 of the coverage area (longitude and latitude computation blocks).

$$r_3 = \sqrt{(x - x_3)^2 + (y - y_3)^2} \tag{3}$$

The coordinates of the radiation sources are determined as follows. Assuming the lightning pulse propagates at the speed of light, C, and using the time difference of arrival of the pulse between any two stations, the difference in distances from the station to the radiation source can be written as:

$$r_2 - r_1 = C^* \Delta t_{21} \tag{4}$$

$$r_2 - r_3 = C^* \Delta t_{23} \tag{5}$$

$$r_1 - r_3 = C^* \Delta t_{13} \tag{6}$$

In the above, Δt_{21} is the difference in arrival times of the pulses between antennas 1 and 2. Δt_{23} and Δt_{13} are the time differences of arrival between stations 2–3 and 1–3, respectively. Substituting the equations for r_1, r_2, and r_3, we get:

$$\sqrt{(x - x_2)^2 + (y - y_2)^2} - \sqrt{x^2 + y^2} = C^* t_{21} \tag{7}$$

$$\sqrt{(x - x_2)^2 + (y - y_2)^2} - \sqrt{(x - x_3)^2 + (y - y_3)^2} = C^* t_{23} \tag{8}$$

$$\sqrt{x^2 + y^2} - \sqrt{(x - x_3)^2 + (y - y_3)^2} = C^* t_{13} \tag{9}$$

The above nonlinear equations can be solved for x and y by using numerical techniques. Eq. (7) to Eq. (9) can be expanded to two equations to obtain the final result of the TDOA method. Because of the fact that only three sensors are used, the computed answers will give two strike location solutions (the true lightning strike point and the false strike point). In this research, a developed TDOA computation program computed both the true and false points generated by the three hyperbola equations.

3. Hardware installation

Lightning location systems typically encompass many sensors, with spatial distances up to hundreds of kilometres. The current research used the data captured by three installed stations at Universiti Teknologi Malaysia, Johor, Malaysia. The coordinates of the stations were (1.560447, 103.643542) for the IVAT Station, (1.557839, 103.635694) for the B11 Station, and (1.565997, 103.633469) for the VAN station. These created between 1 and 2 km distances between the stations. It should be noted that, in practice, there are distance related limitations in the installation of the measuring stations as the LLS based on the TDOA

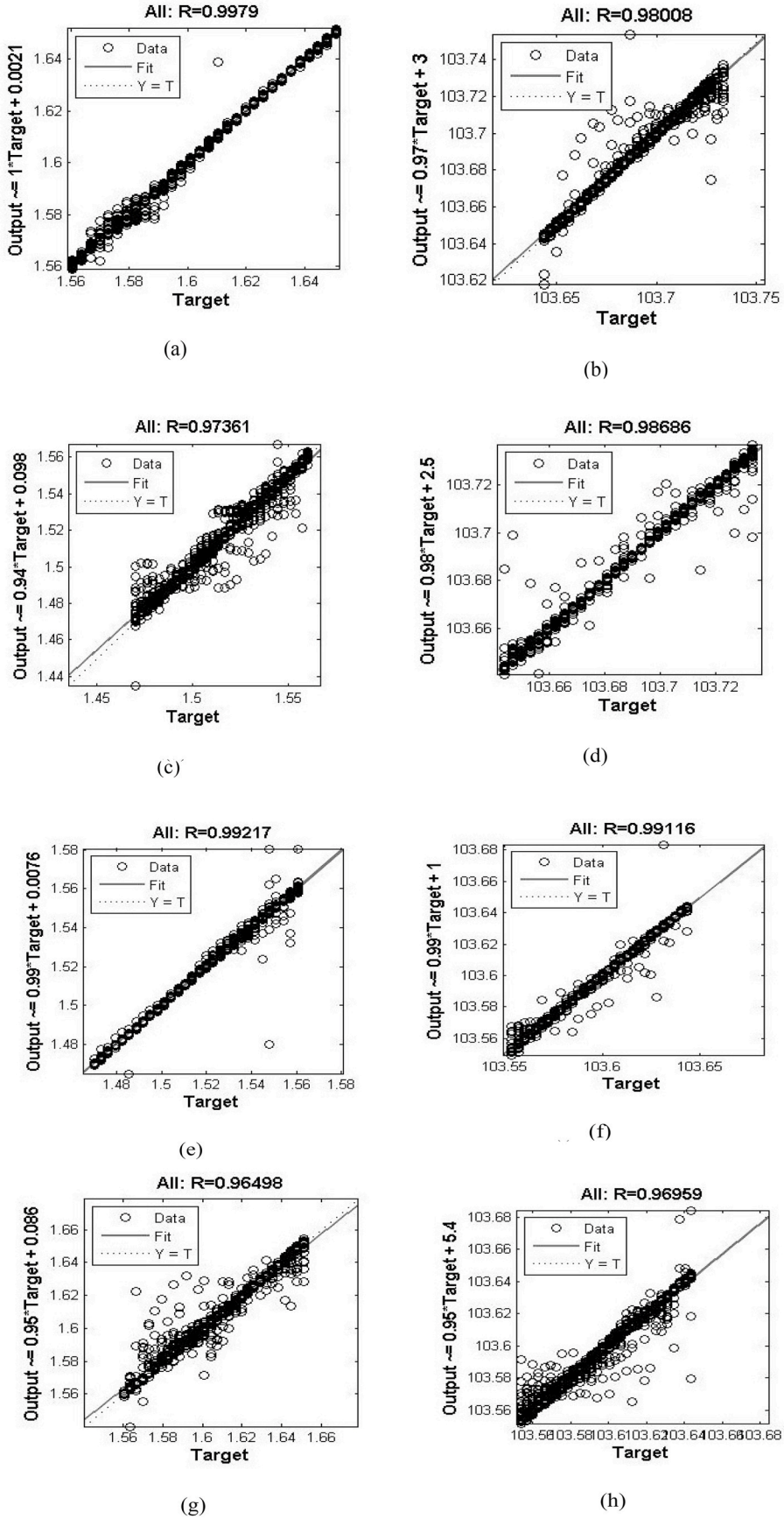

Fig. 9. Regression plots of trained ANNs for quadrant 1 ((a) latitude computation block, (b) longitude computation block), for quadrant 2 ((c) latitude computation block, (d) longitude computation block), for quadrant 3 ((e) latitude computation block, (f) longitude computation block), for quadrant 4 ((g) latitude computation block, (h) longitude computation block).

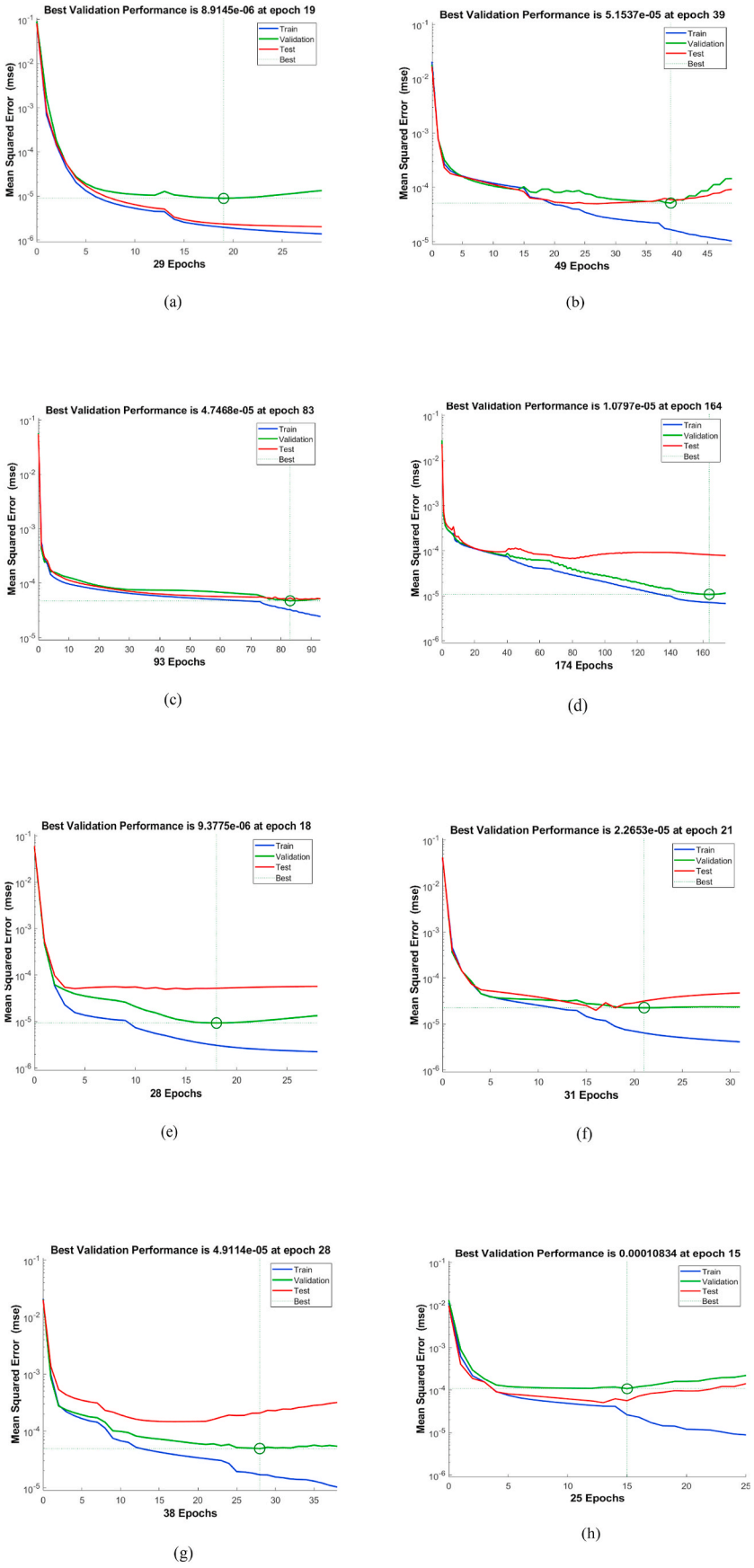

Fig. 10. Performance plots of trained ANNs for quadrant 1, (a) latitude computation block and (b) longitude computation block, for quadrant 2, (c) latitude computation block and (d) longitude computation block, for quadrant 3, (e) latitude computation block and (f) longitude computation block, and for quadrant 4, (g) latitude computation block and (h) longitude computation block.

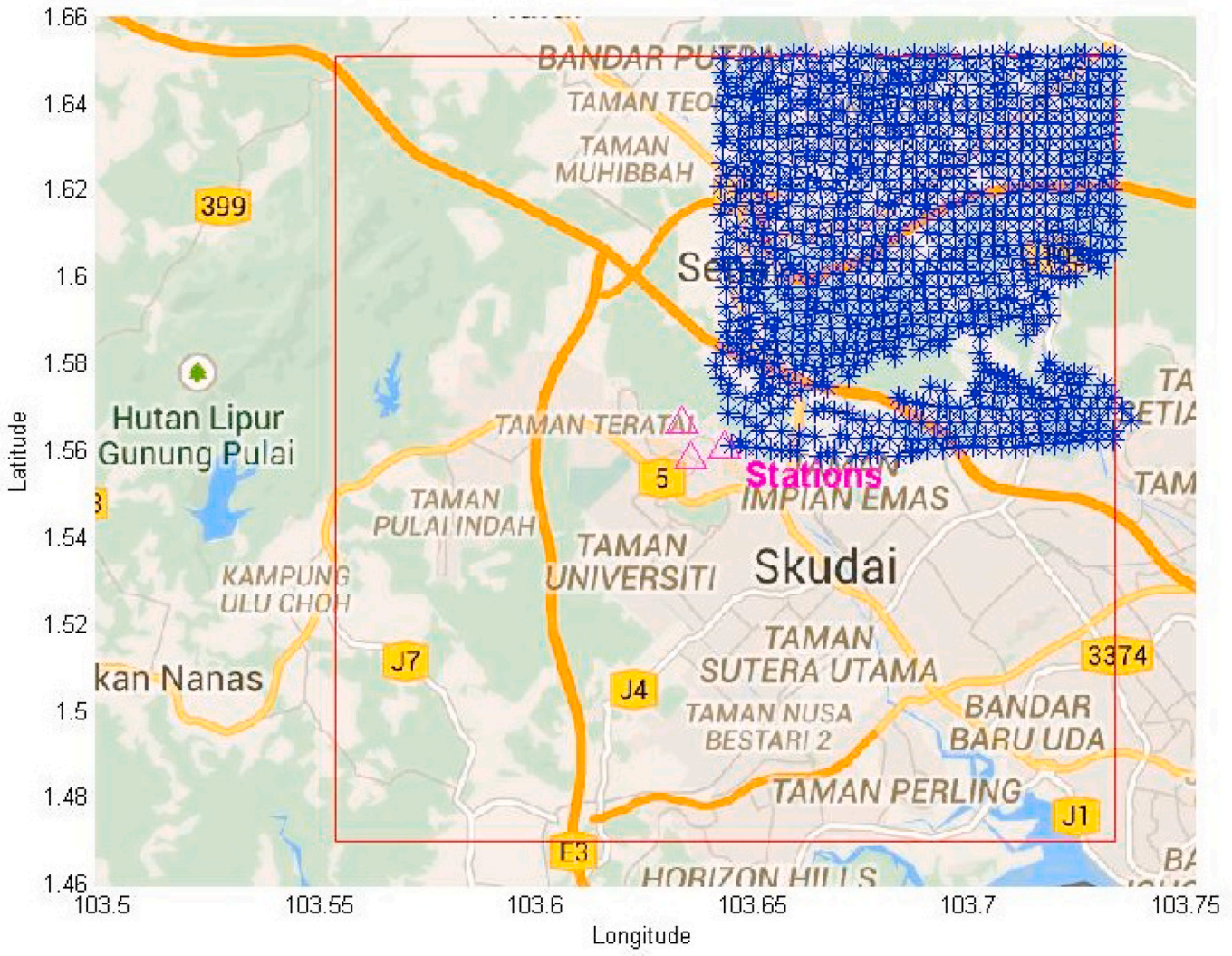

Fig. 11. ANN outputs of simulated input points in quadrant 1, where distances with input points are less than 500 m.

method would fail to detect the lightning strikes close to the stations. This is due to the limited precision of the GPS cards which would save almost similar timestamps, and hence no detectable time difference (Mehranzamir et al., 2018).

Highly accurate GPS cards with nanosecond precision were employed in the current research to increase the accuracy of the LLS in close lightning activities. Even though all stations would capture almost similar timestamps, there is still detectable difference in the last three digits of the timestamps. Fig. 3 shows the locations of the measurement sensors. The X and Y axes express the longitude and latitude, respectively, in the geographic coordinate system. All three sets of lightning location sensors were first installed at the server station (IVAT) for calibration before being placed at their respective stations (IVAT, B11 and VAN). The objective of the calibration test was to ensure that the prepared hardware and equipment for all stations were identical.

A localised LLS operates according to the detected lightning strike by using installed stations within a coverage area. An area of 400 km^2, with a central point at the IVAT station, was selected as the coverage area for the current LLS. The longitude and latitude values of the four vertices of the coverage area were (1.469982–103.553678), (1.650912–103.553678), (1.469982–103.733406), and (1.650912–103.733406).

It should be emphasized that the location of the stations has a direct influence not only on the ANN training but also on the TDOA mathematical calculations in a three-station LLS. Therefore, the ANN engine was trained based on the fixed inputs including the positions of the measuring stations. A new set of training would be required if the LLS system is to be installed in other locations.

The TDOA method was based on the timestamps detected by the GPS antennas. As noted above, the GPS is a space-based satellite navigation system that provides location and time information in all weather conditions. Three GPS cards (GPS180PEX) were used at each station for time synchronisation and for saving the timestamps with the highest precision. Images of the GPS card and its antenna are presented in Fig. 4. The PCI Express slot card was the best choice for adding a highly accurate time base to the control stations. The GPS180PEX is a low-profile board for computers with a PCI express interface. The rear slot cover integrated the antenna connector, a BNC connector for modulated time codes, a 9 pin D_SUB male connector, and two status LEDs. The resolution of the pulse outputs was 100 ns (Mehranzamir, 2015).

When the incoming signal passed the threshold, the GPS was consequently triggered by the PicoScope software via the RS-232 port on the GPS card. An executable file was generated based on Microsoft Visual Studio software and 'C' language programming. The program saved the timestamp at each station with a specified format and file name. Three examples of the saved timestamp lines related to the waveforms captured at the stations are as follows: 06_10_18_08_43_32.1728546, 06_10_18_21_59_1.6345212, and 25_08_18_10_28_08_7,444,817. In the first example, 06 represents the day, 10 the month (October), 18 the year

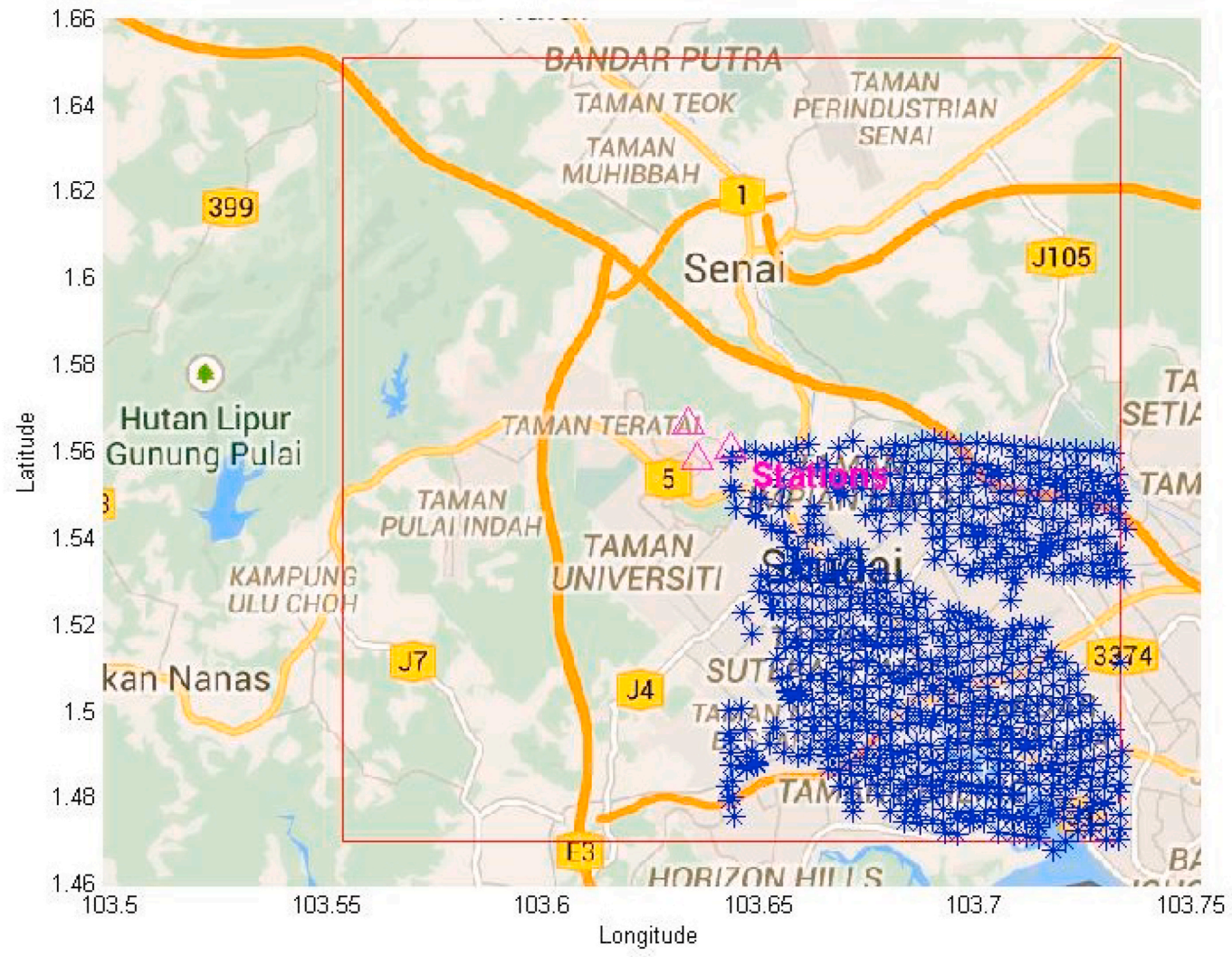

Fig. 12. ANN outputs of simulated input points in quadrant 2, where distances with input points are less than 500 m.

(2018), 08 the hour, 43 the minute, 32 the second, and 1,728,546 the seven decimal places of the second.

4. Application of artificial neural network

ANN is a subdivision of the concept of artificial intelligence. ANN scheme is based on the processes of a biological neural network, and is defined as an imitation of biological neural systems. ANN is an intelligent machine learning technique, and its historical development can be traced back to 1943 (Sivanandam and Deepa, 2006). In recent years, neural networks have had significant functions in engineering sectors and industrial applications. ANN is trained by input examples to find patterns and correlations between inputs and outputs. The trained network is essentially suitable for pattern recognition and forecasting. ANN adjusts itself when inputs and outputs are injected to the algorithm (Bates et al., 2018; Silva et al., 1999).

ANN has several significant and useful advantages. For example, ANN can achieve tasks that a linear program cannot, and it also does not require reprogramming. In addition, ANN can be applied to any request in any problematic sector. However, ANN also have numerous difficulties, such as the requirements for training to properly function, and the need for high processing periods for large networks. To control the best ANN model, numerous feed-forward back-propagation ANN schemes have been created, and each network presentation can be assessed by using a cross-validation method.

The ANN model with the best performance is designated as the best for a given project. Owing to its high accuracy, high computational speed, and great efficiency, several researchers have used ANN in lightning studies for LLSs and lightning predictions, lightning model evaluations, and storm forecasting (Bala et al., 2017; Choudhury et al., 2004; Ekonomou et al., 2006; Gardner and Dorling, 1998; Johari et al., 2010; Maqsood et al., 2005; McCann, 1992). Kenneth Levenberg and Donald Marquardt developed the Levenberg–Marquardt algorithm that provides a numerical solution to the problem of minimising a nonlinear function. This method is fast and has stable convergence, and is suitable for training small- and medium-size problems (Ekonomou et al., 2007; Marquardt, 1963; Reynaldi et al., 2012; Sathya and Abraham, 2013; Valero et al., 2010; Yu and Wilamowski, 2011).

As explained above, the main step in a TDOA calculation is solving the intersection points of the hyperbolas. In this study, the TDOA computation block formed and solved the hyperbola equations based on the three stations. To employ the ANN to detect the location of lightning, 3600 input sample points were assumed as lightning points to train the ANN engine, as shown in Fig. 5. Hence, according to the TDOA block, there are one true strike point and one false strike point. The training process of the neural network requires several inputs as samples to extract the best pattern of the network using the ANN algorithm.

The longitudes and latitudes of the stations were entered into the

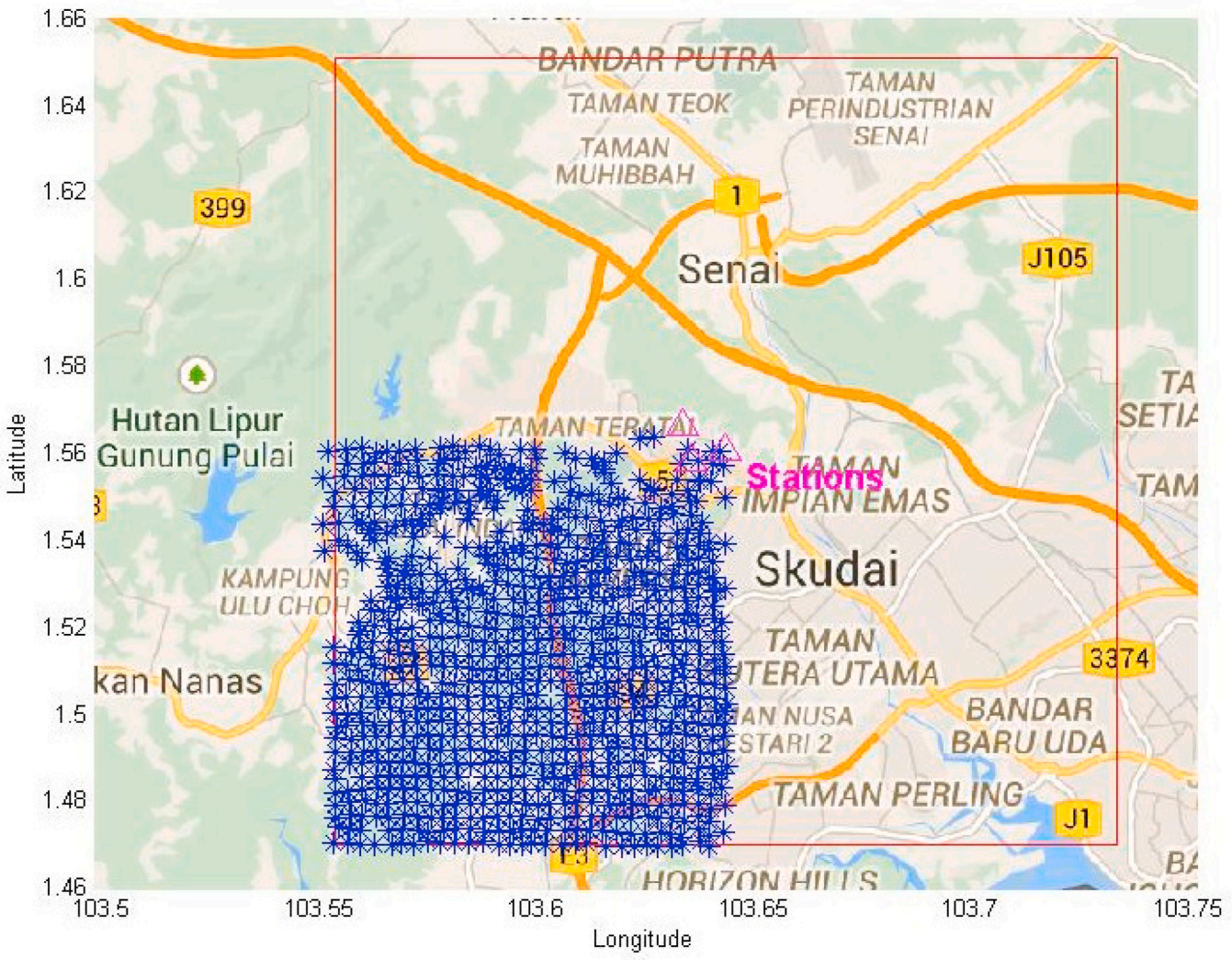

Fig. 13. ANN outputs of simulated input points in quadrant 3, where distances with input points are less than 500 m.

algorithm, and the coverage area was divided into four quadrants (Fig. 6). The coverage area was further divided into points at each quadrant for the TDOA calculations. The results of the ANNs for the TDOA method showed that 3600 input points (considered as lightning strikes) were sufficient for the simulations. It should be indicated that at the first stage of ANN training, the whole coverage area was considered as a single zone. Based on the observations of several trained ANN networks, it was discovered that the accuracy of ANN engines was below the expectations. The configuration of the installed sensors, the number of sensors and the position of the measuring stations with respect to each other, were the major reasons of that low accuracy as there were regions in which the preliminary ANN engine found similar patterns based on the inputs to the ANN block. Therefore, training the whole coverage area as a single network may result in larger errors compared to dividing the area into smaller quadrants. The results of training the ANN engine in different quadrants have demonstrated the truth of this idea.

The next step was to constitute hyperbola equations obtained from the three-station configuration. As previously stated, using three stations would lead to a false strike point in addition to the true one. The true and false points of all inputs (3600 points) were saved in the TDOA computation block. A flowchart of the TDOA calculations for all four quadrants in the coverage area is illustrated in Fig. 7.

5. Artificial neural network training

The neural network has the ability to learn from the environment and improve its performance by learning. The environment or dynamic systems can teach the ANN to learn by iterative process of adjustments applied to its weight and biases. A set of exemplars, which is typically a group of patterns of available environmental variables, characterize the environment. The network will become more knowledgeable about its environment after several iterations during the learning process. ANN learning is almost similar to learning by humans, where an inferred process cannot be perceived directly. The neural network architecture is determined by the number of layers, the number of nodes or neuron units in each layer, and the weighted connections between nodes. The number of layers includes the input layer, hidden layers, and the output layer. In this work, an ANN was used to determine the true lightning strike point from two given solutions, and the Levenberg–Marquardt algorithm was selected as the ANN training algorithm.

Fig. 8 presents the flowchart of the training process of the proposed algorithm for extracting the true lightning strike in both the longitude and latitude computation blocks. In the longitude computation block, the longitude of the true point was selected from two solutions, and the latitude computation block individuated the latitude of the true point using the trained neural networks. To form the neural networks, the vertices and coordinates of the quadrants and stations were first

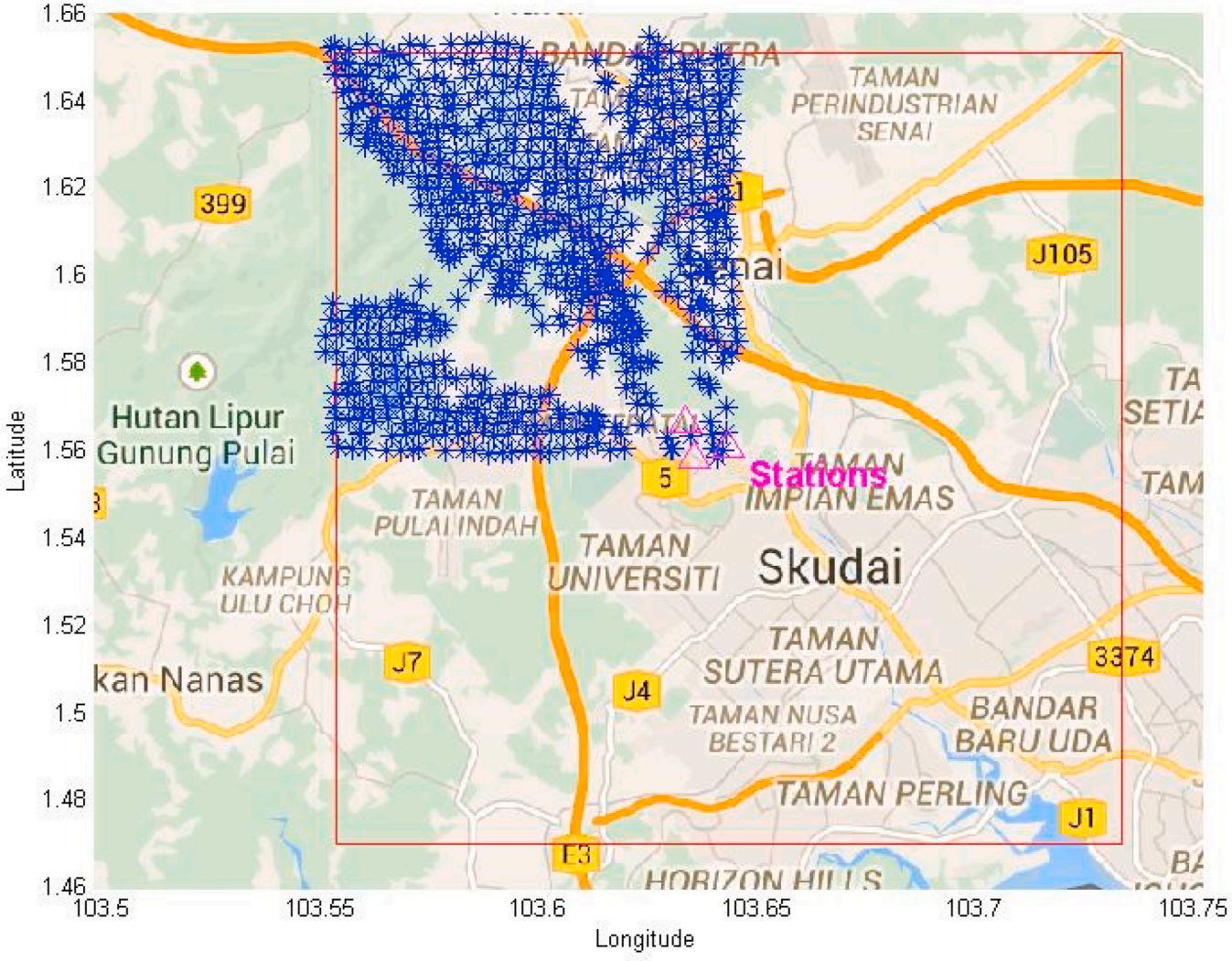

Fig. 14. ANN outputs of simulated input points in quadrant 4, where distances with input points are less than 500 m.

Table 1
Statistical analysis of simulated input points and artificial neural network (ANN) output results in four quadrants using time difference of arrival (TDOA) method.

Statistical Parameters	Quadrant 1	Quadrant 2	Quadrant 3	Quadrant 4
Mean (differences of latitudes)	0.00080252	0.003386	0.00099328	0.002727
Mean (differences of longitudes)	0.001790	0.001399	0.001202	0.003186
Mean (differences of calculated distances (m))	231	449	197	520
Median (differences of calculated distances (m))	81	204	73	228
SD (differences of calculated distances (m))	574	700	504	930

Table 2
Number of input points and ANN output points in the coverage area, wherein distances between input and output points are greater than 500 m.

Quadrant	Number of locations (latitude, longitude)
Quadrant 1	82 points out of 900
Quadrant 2	213 points out of 900
Quadrant 3	61 points out of 900
Quadrant 4	208 points out of 900

uploaded to the network. Then, the results of the TDOA computation block (Fig. 7) were uploaded as the main parameters, known as INPUT to the ANN algorithm.

The inputs for training the ANN were the two true and false points, distances between the true and false points, and angles between the two points as presented in a matrix in Eq. (10). The time difference between the detected timestamps at IVAT and B11 stations for the first solution or answer is $\Delta t_{TDOA(IVAT-B11)_1}$, whereas $\Delta t_{TDOA(IVAT-B11)_2}$ is the time difference between the IVAT and B11 stations for the second TDOA result. The distance between the two results of the TDOA method for the incoming signal is $\Delta R_{answer\ 1\ to\ answer\ 2}$ and finally, $Angle_{answer\ 1\ to\ answer\ 2}$ is the angle between the two TDOA results. The INPUT array comprised of 3600 samples, as imagined lightning strikes within the coverage area. The training process was performed in two computation blocks for each quadrant, one for the longitude and one for the latitude. After quadrant 1, the ANN training process was then repeated for quadrants 2 to 4.

$$\begin{bmatrix} \Delta t_{TDOA(IVAT-B11)_1} * C & \Delta t_{TDOA(IVAT-B11)_2} * C \\ \Delta t_{TDOA(B11-VAN)_1} * C & \Delta t_{TDOA(B11-VAN)_2} * C \\ \Delta t_{TDOA(IVAT-VAN)_1} * C & \Delta t_{TDOA(IVAT-VAN)_2} * C \\ \Delta R_{answer1toanswer2} & Angle_{answer1toanswer2} \end{bmatrix} \quad (10)$$

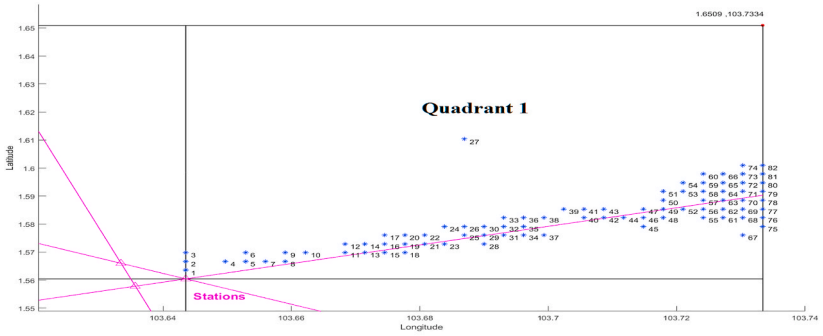

(a)

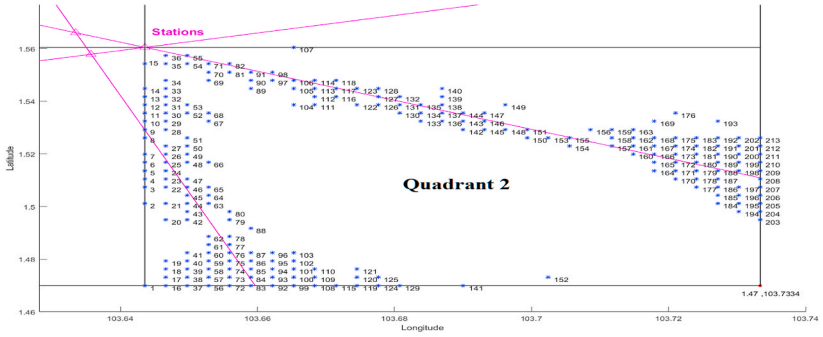

(b)

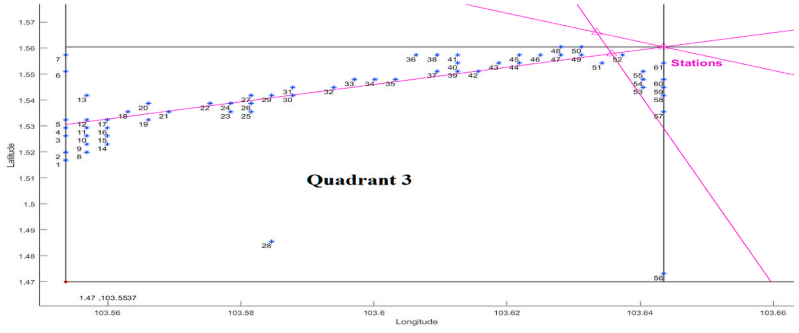

(c)

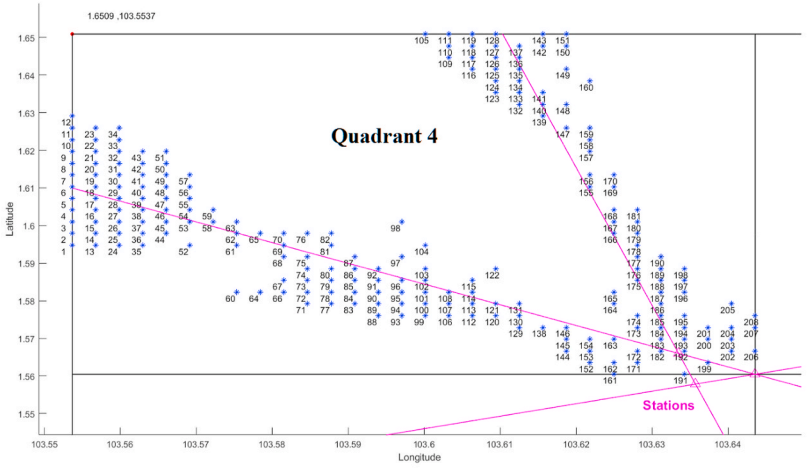

(d)

Fig. 15. Simulated input points in the coverage area, wherein distances with its correlated outputs are greater than 500 m (see Table 2) in (a) Quadrant 1, (b) Quadrant 2, (c) Quadrant 3, and (d) Quadrant 4.

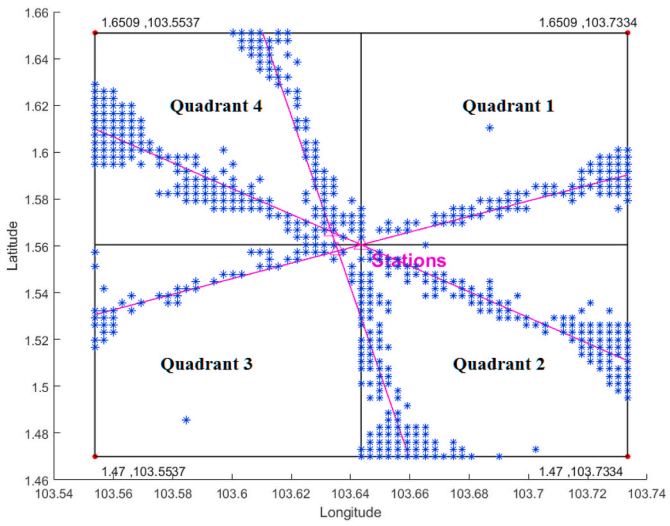

Fig. 16. Simulated input points wherein distances with ANN outputs are greater than 500 m (integration of Fig. 15(a–d)).

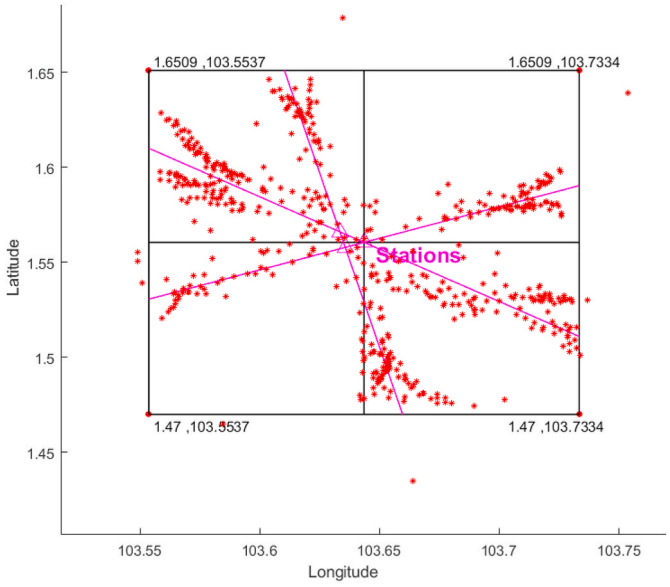

Fig. 17. ANN output points wherein distances with simulated input points in Fig. 16 are greater than 500 m (latitude and longitude of the red stars are tabulated in Appendix).

6. Results and discussion

The two neural networks (longitude and latitude computation blocks) for the four quadrants were trained and then were tested within the coverage area. The regressions for the latitude and longitude were 0.9979 and 0.98008 for quadrant 1, 0.97361 and 0.98686 for quadrant 2, 0.99217 and 0.99116 for quadrant 3, and 0.96498 and 0.96959 for quadrant 4, as shown in Fig. 9. The regression plot is used to quantify the relationship between a target value and an output variable. In other words, the ANN's regression plots anticipate outputs as a function of the inputs. The aim of regression analysis is to generate a line that best fits the input data. However, the outputs will never fit precisely on the line and the best-fitted line is plotted with the least amount of dispersion points around the line.

The network memorised the specific training samples. All plots in Fig. 9 do not indicate any major problems with the training. The X axes in Fig. 9(a), (c), 9(e), 9(g) are the target latitudes which were desired to be achieved by the LATITUDE block while the Y axes are the output of the ANN engines in this block. The 45-degree line of regressions is so named because it forms a 45-degree angle with both X and Y axes when plotted by the ANN engines. These regression lines are used to showcase the correlation between Targets and Outputs in this training as a means of identifying equilibrium. In like manner, the Y axes in Fig. 9(b), (d), 9 (f), 9(h) are the output longitudes which were expected to be achieved by the LONGITUDE block while the X axes are the Targets in this block. Once more, the regression plots follow a 45-degree line which represent an acceptable equilibrium between TARGETs and OUTPUTs of the LONGITUDE block.

The performance values of the train, validation, and test engines of the trained network for the longitude and latitude computation blocks (in all quadrants) are presented in Fig. 10. The data displayed in Fig. 10 indicates the iteration at which the performance error reaches a minimum, and this epoch is known as the best, that is where the training engine achieves the best condition. The engine training was conducted using a set of 39 (for longitude) and 19 (for latitude) iterations. After the 39th and 19th iterations in quadrant 1, the training was continued for additional iterations, before it finally stopped at 49th iteration (for longitude) and 29th iteration (for latitude).

In quadrant 2, the engine training was conducted with a set of 164 (for longitude) and 83 (for latitude) iterations. After the 164th and 83rd iterations, the training was continued for additional iterations, before finally stopping at 174th iteration (for longitude) and 93rd iteration (for latitude). In quadrant 3, the engine training was conducted using a set of 21 (for longitude) and 18 (for latitude) iterations. After the 21st and 18th iterations, the training was continued for additional iterations before finally stopping at 31st iteration (for longitude) and 28th iteration (for latitude). In quadrant 4, the engine training was conducted using a set of 15 (for longitude) and 28 (for latitude) iterations. After the 15th and 28th iterations, the training was continued for additional iterations, before finally stopping at 25th iteration (for longitude) and 38th iteration (for latitude).

6.1. Validation of trained longitude and latitude computation blocks in quadrant 1

The longitude and latitude neural networks for quadrant 1 were trained in the last section. A set of 900 points were then selected to test the trained ANN in quadrant 1. These 900 points were entered to longitude and latitude computation blocks as ANN inputs, which were considered as lightning strikes. Fig. 11 presents the ANN output points for selected inputs, where the distance differences between the input and ANN output points were less than 500 m.

6.2. Validation of trained longitude and latitude computation blocks in quadrant 2

The longitude and latitude neural networks for quadrant 2 were trained in the last section. A set of 900 points were then selected to test the trained ANN in quadrant 2. Fig. 12 shows the ANN output points for selected inputs, where the distance differences between the inputs and ANN output points were less than 500 m.

6.3. Validation of trained longitude and latitude computation blocks in quadrant 3

The longitude and latitude neural networks for quadrant 3 were trained in the last section. A set of 900 points were then selected to test the trained ANN in quadrant 3. Fig. 13 presents the ANN output points for selected inputs, where the distance differences between the input and output points were less than 500 m.

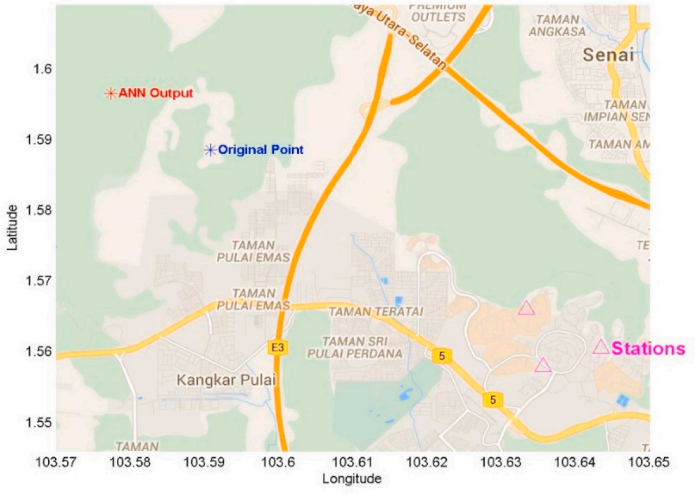

(a)

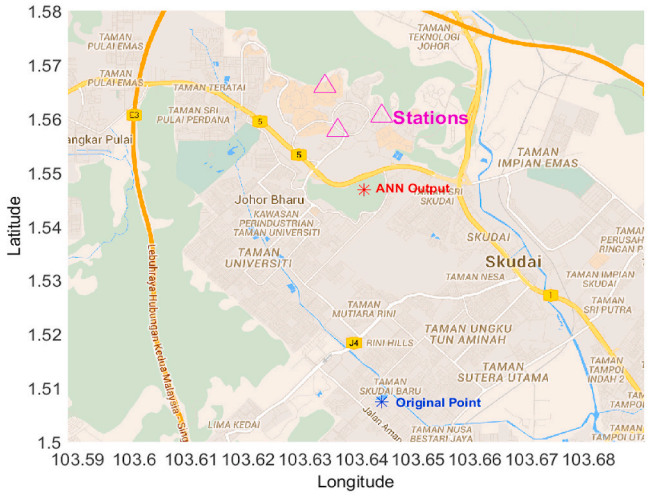

(b)

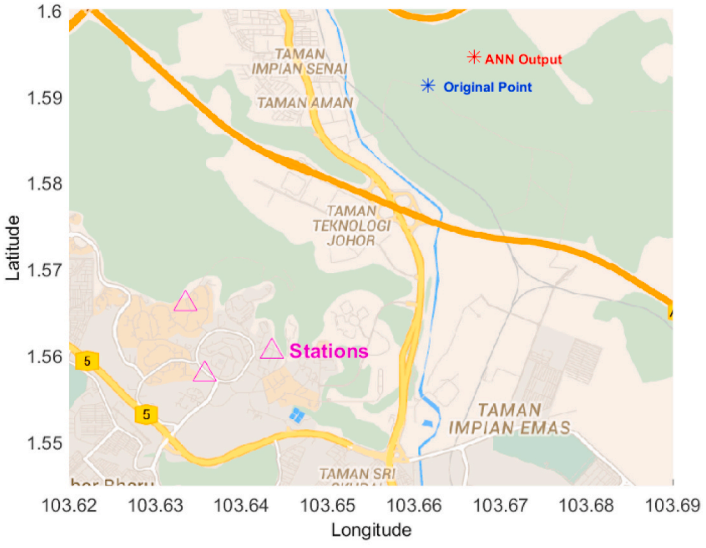

(c)

Fig. 18. Three samples of close-up views of lightning discharge original points and ANN outputs in Fig. 11–16.

6.4. Validation of trained longitude and latitude computation blocks in quadrant 4

The longitude and latitude neural networks for quadrant 4 were trained in the last section. A set of 900 points were then selected to test the trained ANN in quadrant 4. Fig. 14 shows the ANN output points for selected inputs, where the distance differences between the input and output points were less than 500 m.

6.5. Statistical analysis

The simulation results in all four quadrants indicated that the trained ANNs for the TDOA method were able to find the correct lightning discharge point between the true and false answers. It should be noted here that, these results (output points) have distance errors, which are dependent on the location of the strike points in the coverage area. The statistical analysis of the output results including Mean and Median differences between the longitudes and latitudes of the inputs and the ANN outputs and Standard Deviation (SD) are given in Table 1.

The Mean differences of the calculated distances in quadrants 3 and 1 were 197 m and 231 m, respectively, which were the best among the four quadrants. In quadrants 2 and 4, the Mean differences of the distances were 449 m and 520 m, respectively. Thus, quadrant 4 had the largest errors. The Mean differences of latitudes and longitudes in four quadrants identically authenticated the computed Mean differences of distances. Furthermore, the Median differences of calculated distances were also computed in four quadrants. The Median number in a series of data is found by ordering all points and picking out the one in the middle. In the case where there are two middle numbers, the Mean of those two numbers is taken. The Median differences of calculated distances were 81 m, 204 m, 73 m and 228 m in quadrants 1, 2, 3 and 4, respectively. The greater difference between the Mean and Median in a dataset demonstrates a skewed distribution. Hence, it can be demonstrated that in quadrants 2 and 4, where the discrepancies between the Mean and Median numbers were 245 m and 292 m respectively, the data points are more distributed around the Means and the Medians. Therefore, there are more distance errors in quadrants 2 and 4. As mentioned above, Median is the value that splits the sorted dataset in half. Thus, the Medians of the calculated distances in quadrants 1 and 3 indicated that 50% of data had distance error of less than 81 m and 73 m respectively. Standard Deviation (SD) by definition is the measure of dispersion of a dataset from its Mean value. In other words, it is a measure of the average distance between the values of the points in the dataset and the Mean. In this study, the sample size of the validation test was 3600 points in all quadrants. The calculated SD values were 574 m, 700 m, 504 m and 930 m in quadrants 1, 2, 3 and 4, respectively. As it was expected, the SD values in quadrants 4 and 2 were higher than those in quadrants 1 and 3. The SD will be low if the values in the dataset are almost similar while the SD will be high if the values in the dataset are highly variable.

In order to comprehend the causes of significant discrepancies among the Median values and the Means in all four quadrants, distance differences of 500 m between the assumed input points and ANN output points (see Figs. 11–14) are selected as margins. The number of the input points and ANN output points wherein the distance differences between inputs and outputs locations were greater than 500 m are tabulated in Table 2. These locations had the main contributions in creation of large Mean differences of calculated distances. Also, the considerable gaps between the Medians and Means are affected by these data points.

The input points to the ANN engines in quadrants 1 to 4 which were counted in Table 2 are illustrated in Fig. 15. A total number of 82, 213, 61 and 211 input points out of 900 sample points at each quadrant had distances differences greater than 500 m with their correlated ANN output points. The stations are shown by Δ in Fig. 15 and the lines in magenta colour are the lines that pass through two stations simultaneously. The borders of the coverage area and quadrants' boundaries are drawn in black colour.

Fig. 16 is plotted by integrating four figures in Fig. 15 to perceive the behaviour of the LLS in this study. Moreover, Fig. 17 presents the ANN output points of the system where distances with the input points are greater than 500 m in the coverage area. There are short distances or overlap between many red stars (output points) in some areas in Fig. 17. Therefore, labelling the ANN output points inside Fig. 17 with their correlated numbers of input points in Fig. 15 (a)–(d) was unrecognizable and obscure. To solve this problem, the longitude and latitude of the input points, output points, and the label of correlated input points are tabulated in Appendix. Besides, the distances between input points and output results of the locations in Table 2 and Fig. 15 are presented in front of each point in the Appendix. The plotted red stars in Fig. 17 have correlation with ANN inputs in Fig. 15 (a)–(d) and obviously the blue stars in Fig. 16.

It is evident from Figs. 16 and 17 that in quadrants 2 and 4, the distance errors greater than 500 m (between the input points and ANN outputs) occurred in two areas, while in quadrants 1 and 3, the Mean errors were lower than those in quadrants 2 and 4. By referring to the drawn magenta colour lines in Fig. 15, it was clear that the distance errors greater than 500 m mostly occurred around the lines which pass through two stations simultaneously, and this problem is inevitable in a three-station TDOA-based LLS.

To clarify the distances between the input points (original lightning discharge) and ANN outputs of the proposed longitude and latitude computation blocks, close-up views of three samples in Figs. 11–15 are illustrated in Fig. 18.

7. Conclusion

Weather forecasting companies, research institutes, power networks, and insurance companies are common owners of LLSs. Industrial LLSs utilize several measuring stations, which are massive in size and overly expensive. The number of measuring stations in an LLS has direct relations to the reliability and accuracy of the system in locating a lightning discharge with the lowest uncertainty. The small differences in the arrival times of lightning discharges at different synchronized measuring stations are employed in the TDOA method to determine the strike location. Improvements can still be made to LLSs, especially those using the TDOA technique, including reducing the number of sensor station to a minimum to save cost. For TDOA, using three sensor stations may lead to two solutions, a true and a false strike point. An ANN algorithm was proposed to determine the true strike point. The algorithm was tested on site with the coverage area being divided into four quadrants. The mean errors of the ANN assisted TDOA-based LLS were 231, 449, 197, and 520 m for quadrants 1 to 4, respectively, giving an average error of approximately 350 m. The algorithm has helped the three-station TDOA-based LLS to successfully locate the lightning strike point with a notable accuracy comparable to that of commercial systems.

Declaration of competing interest

The authors declare that they have no known competing financial interests or personal relationships that could have appeared to influence the work reported in this paper.

Acknowledgment

Authors wish to thank Universiti Teknologi Malaysia for the funding of the research (grant numbers 02M18, 05G88 and 01M44).

Appendix

Quadrant 1					
Input point number presented in Fig. 15(a)	Input points in Fig. 15 (a)		ANN output points in Fig. 17		Distances between input points and ANN output points (m)
	Latitude	Longitude	Latitude	Longitude	
1	1.5635667	103.6435388	1.5637661	103.6176458	2876
2	1.5666618	103.6435388	1.5667651	103.6231801	2261
3	1.5698143	103.6435388	1.5622154	103.6436102	844
4	1.5666618	103.6497267	1.5631150	103.6354008	1639
5	1.5666618	103.6528207	1.5727357	103.6771645	2787
6	1.5698143	103.6528207	1.5673956	103.6463871	764
7	1.5666618	103.6559147	1.5687396	103.6610673	617
8	1.5666618	103.6590086	1.5736959	103.6881891	3334
9	1.5698143	103.6590086	1.5729088	103.6667372	925
10	1.5698143	103.6621599	1.5775396	103.6976208	4031
11	1.5698143	103.6683478	1.5773918	103.7050179	4159
12	1.5729094	103.6683478	1.5773113	103.6838169	1787
13	1.5698143	103.6714418	1.5740405	103.6772145	795
14	1.5729094	103.6714418	1.5799676	103.7034128	3637
15	1.5698143	103.6745358	1.5729808	103.6781989	538
16	1.5729094	103.6745358	1.5672498	103.6758739	646
17	1.5760619	103.6745358	1.5794962	103.6818111	894
18	1.5698143	103.6776298	1.5728495	103.6818502	578
19	1.5729094	103.6776298	1.5791555	103.7129125	3980
20	1.5760619	103.6776298	1.5802213	103.6939644	1872
21	1.5729094	103.6807237	1.5761655	103.6876197	847
22	1.5760619	103.6807237	1.5821587	103.7068555	2981
23	1.5729094	103.6838177	1.5763497	103.6915439	940
24	1.5791570	103.6838177	1.5814525	103.6918441	927
25	1.5760619	103.6869117	1.5801698	103.7173473	3411
26	1.5791570	103.6869117	1.5840602	103.7057919	2167
27	1.6103380	103.6869117	1.6390925	103.7537454	8082
28	1.5729094	103.6900056	1.5753714	103.6956298	682
29	1.5760619	103.6900056	1.5779809	103.6976465	875
30	1.5791570	103.6900056	1.5850213	103.7091048	2219
31	1.5760619	103.6930996	1.5783293	103.6998601	792
32	1.5791570	103.6930996	1.5791130	103.7018812	975
33	1.5823095	103.6930996	1.5849408	103.7018339	1013
34	1.5760619	103.6961936	1.5781308	103.7029744	787
35	1.5791570	103.6961936	1.5801929	103.7147433	2064
36	1.5823095	103.6961936	1.5859513	103.7110462	1699
37	1.5760619	103.6993449	1.5776670	103.7049687	650
38	1.5823095	103.6993449	1.5863972	103.7102885	1298
39	1.5854046	103.7024388	1.5871782	103.7093854	796
40	1.5823095	103.7055328	1.5806284	103.7132322	875
41	1.5854046	103.7055328	1.5864769	103.7119570	723
42	1.5823095	103.7086268	1.5793628	103.7048687	531
43	1.5854046	103.7086268	1.5864564	103.6960374	1403
44	1.5823095	103.7117208	1.5792256	103.7074828	582
45	1.5791570	103.7148147	1.5767783	103.7100326	593
46	1.5823095	103.7148147	1.5787568	103.7092761	731
47	1.5854046	103.7148147	1.5812255	103.7125557	528
48	1.5823095	103.7179087	1.5784328	103.7107476	905
49	1.5854046	103.7179087	1.5786333	103.6997486	2153
50	1.5884998	103.7179087	1.5901015	103.7086308	1046
51	1.5916523	103.7179087	1.5890675	103.7136247	556
52	1.5854046	103.7210027	1.5798453	103.7108272	1288
53	1.5916523	103.7210027	1.5892516	103.7161219	604
54	1.5947474	103.7210027	1.5930292	103.7162140	565
55	1.5823095	103.7240966	1.5779120	103.7142810	1195
56	1.5854046	103.7240966	1.5794562	103.7123063	1467
57	1.5884998	103.7240966	1.5830048	103.7140422	1273
58	1.5916523	103.7240966	1.5898323	103.7167510	841
59	1.5947474	103.7240966	1.5923416	103.7182824	699
60	1.5978999	103.7240966	1.5961883	103.7195260	542
61	1.5823095	103.7271906	1.5798181	103.7225512	585
62	1.5854046	103.7271906	1.5813085	103.7197025	948
63	1.5884998	103.7271906	1.5782046	103.6965011	3596
64	1.5916523	103.7271906	1.5864394	103.6745289	5878
65	1.5947474	103.7271906	1.5919377	103.7201760	839
66	1.5978999	103.7271906	1.5952872	103.7206450	783
67	1.5760619	103.7302846	1.5742332	103.7261111	506
68	1.5823095	103.7302846	1.5797775	103.7247023	681
69	1.5854046	103.7302846	1.5812026	103.7218735	1044
70	1.5884998	103.7302846	1.5794472	103.7075183	2722
71	1.5916523	103.7302846	1.5905005	103.7100530	2251

(continued on next page)

(*continued*)

Quadrant 1					
Input point number presented in Fig. 15(a)	Input points in Fig. 15 (a)		ANN output points in Fig. 17		Distances between input points and ANN output points (m)
	Latitude	Longitude	Latitude	Longitude	
72	1.5947474	103.7302846	1.5907759	103.7190457	1324
73	1.5978999	103.7302846	1.5945516	103.7219045	1002
74	1.6009951	103.7302846	1.5987241	103.7250734	631
75	1.5791570	103.7333786	1.5759508	103.7257573	918
76	1.5823095	103.7333786	1.5774427	103.7211493	1462
77	1.5854046	103.7333786	1.5809727	103.7238776	1165
78	1.5884998	103.7333786	1.5819846	103.7193857	1715
79	1.5916523	103.7333786	1.5834599	103.7115737	2587
80	1.5947474	103.7333786	1.5913865	103.7176875	1782
81	1.5978999	103.7333786	1.5925872	103.7209844	1498
82	1.6009951	103.7333786	1.5977035	103.7256406	934
Quadrant 2					
Input point number presented in Fig. 15 (b)	Input points in Fig. 15 (b)		ANN output points in Fig. 17		Distances between input points and ANN output points (m)
	Latitude	Longitude	Latitude	Longitude	
1	1.4699699	103.6435388	1.4784149	103.6437421	939
2	1.5011493	103.6435388	1.4921965	103.6428787	998
3	1.5073967	103.6435388	1.5027718	103.6429967	517
4	1.5105490	103.6435388	1.4982341	103.6433162	1369
5	1.5136441	103.6435388	1.4993751	103.6435329	1586
6	1.5167964	103.6435388	1.5000653	103.6437790	1859
7	1.5198915	103.6435388	1.5094686	103.6427075	1162
8	1.5261390	103.6435388	1.5088504	103.6429373	1922
9	1.5292340	103.6435388	1.5132490	103.6435234	1776
10	1.5323864	103.6435388	1.5029678	103.6479278	3305
11	1.5354815	103.6435388	1.5043514	103.6518150	3579
12	1.5386339	103.6435388	1.5068465	103.6465876	3548
13	1.5417290	103.6435388	1.5163705	103.6446405	2820
14	1.5448241	103.6435388	1.5574942	103.6407987	1440
15	1.5542240	103.6435388	1.5526217	103.6848329	4590
16	1.4699699	103.6466327	1.4787359	103.6538331	1260
17	1.4731222	103.6466327	1.4806506	103.6477444	846
18	1.4762172	103.6466327	1.4836971	103.6473686	835
19	1.4793122	103.6466327	1.4838332	103.6517603	759
20	1.4949592	103.6466327	1.4892223	103.6474808	644
21	1.5011493	103.6466327	1.4916037	103.6472815	1063
22	1.5073967	103.6466327	1.5018062	103.6464068	622
23	1.5105490	103.6466327	1.5030484	103.6474137	838
24	1.5136441	103.6466327	1.4883737	103.6491573	2822
25	1.5167964	103.6466327	1.4883244	103.6497657	3183
26	1.5198915	103.6466327	1.4900083	103.6507080	3351
27	1.5229866	103.6466327	1.4927898	103.6513964	3397
28	1.5292340	103.6466327	1.5076942	103.6511814	2446
29	1.5323864	103.6466327	1.5256867	103.6503144	849
30	1.5354815	103.6466327	1.5262507	103.6459332	1029
31	1.5386339	103.6466327	1.5440193	103.6465210	599
32	1.5417290	103.6466327	1.5480881	103.6469422	707
33	1.5448241	103.6466327	1.5668252	103.6447931	2453
34	1.5479765	103.6466327	1.5425279	103.6467896	606
35	1.5542240	103.6466327	1.5546390	103.6991397	5833
36	1.5573191	103.6466327	1.5211088	103.6510117	4053
37	1.4699699	103.6497267	1.4860683	103.6492951	1790
38	1.4731222	103.6497267	1.4885374	103.6500030	1713

(*continued on next page*)

(*continued*)

Quadrant 2					
Input point number presented in Fig. 15 (b)	Input points in Fig. 15 (b)		ANN output points in Fig. 17		Distances between input points and ANN output points (m)
	Latitude	Longitude	Latitude	Longitude	
39	1.4762172	103.6497267	1.4915438	103.6490455	1705
40	1.4793122	103.6497267	1.4924860	103.6485077	1470
41	1.4824645	103.6497267	1.4871592	103.6494617	523
42	1.4949592	103.6497267	1.5016510	103.6499386	744
43	1.4980542	103.6497267	1.4880353	103.6503123	1115
44	1.5011493	103.6497267	1.4887949	103.6507452	1377
45	1.5043016	103.6497267	1.4959602	103.6537459	1029
46	1.5073967	103.6497267	1.4923136	103.6525301	1705
47	1.5105490	103.6497267	1.4975594	103.6542982	1530
48	1.5167964	103.6497267	1.4971049	103.6523411	2207
49	1.5198915	103.6497267	1.5104207	103.6537311	1143
50	1.5229866	103.6497267	1.5090175	103.6510642	1559
51	1.5261390	103.6497267	1.5203959	103.6500920	639
52	1.5354815	103.6497267	1.5403008	103.6493380	537
53	1.5386339	103.6497267	1.5438452	103.6484918	595
54	1.5542240	103.6497267	1.5287808	103.6464278	2851
55	1.5573191	103.6497267	1.5619566	103.6511902	540
56	1.4699699	103.6528207	1.4881780	103.6500010	2047
57	1.4731222	103.6528207	1.4884668	103.6499686	1734
58	1.4762172	103.6528207	1.5021193	103.6503667	2891
59	1.4793122	103.6528207	1.5014656	103.6513713	2467
60	1.4824645	103.6528207	1.4889272	103.6506136	759
61	1.4855595	103.6528207	1.4903234	103.6506572	581
62	1.4887119	103.6528207	1.4978720	103.6539322	1025
63	1.5011493	103.6528207	1.4950847	103.6516814	686
64	1.5043016	103.6528207	1.4928412	103.6532494	1274
65	1.5073967	103.6528207	1.4997779	103.6555514	899
66	1.5167964	103.6528207	1.5119010	103.6534345	548
67	1.5323864	103.6528207	1.5404585	103.6530778	897
68	1.5354815	103.6528207	1.5421256	103.6543363	757
69	1.5479765	103.6528207	1.5527314	103.6547812	571
70	1.5510716	103.6528207	1.5441957	103.6536742	770
71	1.5542240	103.6528207	1.5364832	103.6789679	3510
72	1.4699699	103.6559147	1.5005445	103.6535851	3407
73	1.4731222	103.6559147	1.4911193	103.6516862	2054
74	1.4762172	103.6559147	1.4928014	103.6521599	1889
75	1.4793122	103.6559147	1.4943856	103.6532299	1701
76	1.4824645	103.6559147	1.4937055	103.6541384	1265
77	1.4855595	103.6559147	1.4955002	103.6537614	1130
78	1.4887119	103.6559147	1.4989405	103.6533776	1171
79	1.4949592	103.6559147	1.4896607	103.6578251	626
80	1.4980542	103.6559147	1.4935461	103.6571852	520
81	1.5510716	103.6559147	1.5355936	103.6557729	1720
82	1.5542240	103.6559147	1.5525935	103.6411731	1647
83	1.4699699	103.6590086	1.4946673	103.6542033	2796
84	1.4731222	103.6590086	1.5022665	103.6546847	3274
85	1.4762172	103.6590086	1.5015093	103.6542402	2860
86	1.4793122	103.6590086	1.4819706	103.6546961	563

(*continued on next page*)

(*continued*)

Quadrant 2					
Input point number presented in Fig. 15 (b)	Input points in Fig. 15 (b)		ANN output points in Fig. 17		Distances between input points and ANN output points (m)
	Latitude	Longitude	Latitude	Longitude	
87	1.4824645	103.6590086	1.4766836	103.6603586	660
88	1.4918069	103.6590086	1.4966956	103.6588635	543
89	1.5448241	103.6590086	1.5506148	103.6578273	657
90	1.5479765	103.6590086	1.5359228	103.6579362	1345
91	1.5510716	103.6590086	1.5333874	103.6701491	2322
92	1.4699699	103.6621599	1.4348964	103.6641473	3904
93	1.4731222	103.6621599	1.4791093	103.6606090	687
94	1.4762172	103.6621599	1.4881346	103.6605394	1336
95	1.4793122	103.6621599	1.4906060	103.6606859	1266
96	1.4824645	103.6621599	1.4885878	103.6610620	691
97	1.5479765	103.6621599	1.5283739	103.6770186	2733
98	1.5510716	103.6621599	1.5418475	103.6544117	1338
99	1.4699699	103.6652539	1.4865125	103.6620876	1872
100	1.4731222	103.6652539	1.4838810	103.6632667	1216
101	1.4762172	103.6652539	1.4846229	103.6638432	947
102	1.4793122	103.6652539	1.4858593	103.6644968	732
103	1.4824645	103.6652539	1.4872003	103.6652887	526
104	1.5386339	103.6652539	1.5428555	103.6630892	527
105	1.5448241	103.6652539	1.5314370	103.6733186	1736
106	1.5479765	103.6652539	1.5347698	103.6692551	1533
107	1.5604716	103.6652539	1.5558298	103.6641238	531
108	1.4699699	103.6683478	1.4799332	103.6666969	1122
109	1.4731222	103.6683478	1.4808778	103.6680311	863
110	1.4762172	103.6683478	1.4810418	103.6685795	537
111	1.5386339	103.6683478	1.5432723	103.6681094	516
112	1.5417290	103.6683478	1.5373841	103.6659617	551
113	1.5448241	103.6683478	1.5281857	103.7231016	6357
114	1.5479765	103.6683478	1.5397726	103.6635741	1055
115	1.4699699	103.6714418	1.4781672	103.6713249	911
116	1.5417290	103.6714418	1.5289106	103.6872477	2261
117	1.5448241	103.6714418	1.5317936	103.6715212	1448
118	1.5479765	103.6714418	1.5425825	103.6697124	629
119	1.4699699	103.6745358	1.4760340	103.6742007	675
120	1.4731222	103.6745358	1.4785865	103.6740712	609
121	1.4762172	103.6745358	1.4807494	103.6741711	505
122	1.5386339	103.6745358	1.5316032	103.6716352	845
123	1.5448241	103.6745358	1.5348997	103.6612608	1841
124	1.4699699	103.6776298	1.4761396	103.6774374	686
125	1.4731222	103.6776298	1.4785141	103.6774513	599
126	1.5386339	103.6776298	1.5272779	103.6885260	1749
127	1.5417290	103.6776298	1.5349165	103.6755153	793
128	1.5448241	103.6776298	1.5394081	103.6761716	623
129	1.4699699	103.6807237	1.4756330	103.6802989	631
130	1.5354815	103.6807237	1.5278227	103.6805358	851
131	1.5386339	103.6807237	1.5274018	103.6766825	1326
132	1.5417290	103.6807237	1.5352918	103.6748997	964
133	1.5323864	103.6838177	1.5275575	103.6831680	541
134	1.5354815	103.6838177	1.5250198	103.6929632	1544

(*continued on next page*)

(*continued*)

Quadrant 2					
Input point number presented in Fig. 15 (b)	Input points in Fig. 15 (b)		ANN output points in Fig. 17		Distances between input points and ANN output points (m)
	Latitude	Longitude	Latitude	Longitude	
135	1.5386339	103.6838177	1.5336435	103.6851851	575
136	1.5323864	103.6869117	1.5253328	103.6897841	846
137	1.5354815	103.6869117	1.5296943	103.6948021	1087
138	1.5386339	103.6869117	1.5321353	103.6816630	928
139	1.5417290	103.6869117	1.5385850	103.6933991	801
140	1.5448241	103.6869117	1.5438847	103.6980707	1244
141	1.4699699	103.6900056	1.4745089	103.6895242	507
142	1.5292340	103.6900056	1.5247275	103.6893479	506
143	1.5323864	103.6900056	1.5226520	103.6900372	1082
144	1.5354815	103.6900056	1.5305404	103.6891111	558
145	1.5292340	103.6930996	1.5239198	103.6988938	873
146	1.5323864	103.6930996	1.5311153	103.7061641	1458
147	1.5354815	103.6930996	1.5317105	103.6900149	541
148	1.5292340	103.6961936	1.5199317	103.6812048	1960
149	1.5386339	103.6961936	1.5379049	103.7027775	736
150	1.5261390	103.6993449	1.5225295	103.7070527	945
151	1.5292340	103.6993449	1.5296775	103.7171352	1977
152	1.4731222	103.7024388	1.4778645	103.7023069	527
153	1.5261390	103.7024388	1.5239430	103.7204720	2018
154	1.5229866	103.7055328	1.5205859	103.7110567	669
155	1.5261390	103.7055328	1.5326454	103.7165263	1419
156	1.5292340	103.7086268	1.5318152	103.7048030	513
157	1.5229866	103.7117208	1.5305751	103.7175399	1062
158	1.5261390	103.7117208	1.5302701	103.7151842	599
159	1.5292340	103.7117208	1.5327911	103.7068244	672
160	1.5198915	103.7148147	1.5225366	103.6844943	3381
161	1.5229866	103.7148147	1.5294547	103.7143194	721
162	1.5261390	103.7148147	1.5313031	103.7130669	606
163	1.5292340	103.7148147	1.5320596	103.7185939	524
164	1.5136441	103.7179087	1.5179973	103.7145340	612
165	1.5167964	103.7179087	1.5153127	103.7135596	510
166	1.5198915	103.7179087	1.5299046	103.7164068	1125
167	1.5229866	103.7179087	1.5301149	103.7211526	870
168	1.5261390	103.7179087	1.5311377	103.7187880	564
169	1.5323864	103.7179087	1.5357700	103.7123379	724
170	1.5105490	103.7210027	1.5156806	103.7184037	639
171	1.5136441	103.7210027	1.5184487	103.7222052	550
172	1.5167964	103.7210027	1.5259753	103.7087119	1704
173	1.5198915	103.7210027	1.5294341	103.7181057	1108
174	1.5229866	103.7210027	1.5308639	103.7212888	876
175	1.5261390	103.7210027	1.5322585	103.7205810	682
176	1.5354815	103.7210027	1.5377882	103.7171071	503
177	1.5073967	103.7240966	1.5126201	103.7229644	594
178	1.5105490	103.7240966	1.5165120	103.7233817	667
179	1.5136441	103.7240966	1.5145551	103.7179331	692
180	1.5167964	103.7240966	1.5295657	103.7179011	1577
181	1.5198915	103.7240966	1.5309958	103.7246645	1236
182	1.5229866	103.7240966	1.5311690	103.7212955	961

(*continued on next page*)

(*continued*)

Quadrant 2					
Input point number presented in Fig. 15 (b)	Input points in Fig. 15 (b)		ANN output points in Fig. 17		Distances between input points and ANN output points (m)
	Latitude	Longitude	Latitude	Longitude	
183	1.5261390	103.7240966	1.5335697	103.7192401	986
184	1.5011493	103.7271906	1.5058556	103.7265858	527
185	1.5043016	103.7271906	1.5104260	103.7285445	697
186	1.5073967	103.7271906	1.5141653	103.7254779	776
187	1.5105490	103.7271906	1.5171425	103.7279859	738
188	1.5136441	103.7271906	1.5296801	103.7000590	3501
189	1.5167964	103.7271906	1.5293857	103.7218243	1521
190	1.5198915	103.7271906	1.5303932	103.7294519	1194
191	1.5229866	103.7271906	1.5300348	103.7277060	785
192	1.5261390	103.7271906	1.5331868	103.7212035	1027
193	1.5323864	103.7271906	1.5365797	103.7165022	1275
194	1.4980542	103.7302846	1.5028081	103.7294459	536
195	1.5011493	103.7302846	1.5073556	103.7293751	697
196	1.5043016	103.7302846	1.5117111	103.7284286	849
197	1.5073967	103.7302846	1.5156015	103.7295500	915
198	1.5136441	103.7302846	1.5315279	103.7099063	3012
199	1.5167964	103.7302846	1.5307152	103.7291881	1551
200	1.5198915	103.7302846	1.5304363	103.7299534	1172
201	1.5229866	103.7302846	1.5322290	103.7269590	1091
202	1.5261390	103.7302846	1.5298785	103.7266538	579
203	1.4949592	103.7333786	1.5010116	103.7339058	675
204	1.4980542	103.7333786	1.5046250	103.7322729	740
205	1.5011493	103.7333786	1.5093283	103.7314023	935
206	1.5043016	103.7333786	1.5144179	103.7289637	1226
207	1.5073967	103.7333786	1.5159133	103.7321478	956
208	1.5105490	103.7333786	1.5291795	103.7254325	2251
209	1.5136441	103.7333786	1.5308554	103.7139369	2885
210	1.5167964	103.7333786	1.5301898	103.7366843	1533
211	1.5198915	103.7333786	1.5315188	103.7269272	1477
212	1.5229866	103.7333786	1.5290747	103.7305945	744
213	1.5261390	103.7333786	1.5341139	103.6981542	4012
Quadrant 3					
Input point number presented in Fig. 15 (c)	Input points in Fig. 15 (c)		ANN output points in Fig. 17		Distances between input points and ANN output points (m)
	Latitude	Longitude	Latitude	Longitude	
1	1.5167964	103.5536990	1.5207495	103.5593124	763
2	1.5198915	103.5536990	1.5259279	103.5628663	1219
3	1.5261390	103.5536990	1.5300755	103.5646584	1294
4	1.5292340	103.5536990	1.5335360	103.5639263	1233
5	1.5323864	103.5536990	1.5349945	103.5676427	1576
6	1.5510716	103.5536990	1.5504721	103.5489697	530
7	1.5573191	103.5536990	1.5551814	103.5490132	572
8	1.5198915	103.5567930	1.5236885	103.5618073	699
9	1.5229866	103.5567930	1.5283223	103.5646217	1053
10	1.5261390	103.5567930	1.5319467	103.5664798	1255
11	1.5292340	103.5567930	1.5336545	103.5677719	1315
12	1.5323864	103.5567930	1.5364972	103.5682487	1352
13	1.5417290	103.5567930	1.5393174	103.5509683	700
14	1.5229866	103.5598869	1.5263100	103.5639567	584

(*continued on next page*)

(*continued*)

Quadrant 3					
Input point number presented in Fig. 15 (c)	Input points in Fig. 15 (c)		ANN output points in Fig. 17		Distances between input points and ANN output points (m)
	Latitude	Longitude	Latitude	Longitude	
15	1.5261390	103.5598869	1.5303873	103.5657956	808
16	1.5292340	103.5598869	1.5329416	103.5658479	780
17	1.5323864	103.5598869	1.5342975	103.5701140	1156
18	1.5354815	103.5629809	1.5376979	103.5706546	887
19	1.5323864	103.5660749	1.5345745	103.5703197	531
20	1.5386339	103.5660749	1.5411205	103.5611589	612
21	1.5354815	103.5691689	1.5408535	103.5841574	1769
22	1.5386339	103.5753568	1.5345943	103.5645267	1284
23	1.5354815	103.5784508	1.5333569	103.5737472	573
24	1.5386339	103.5784508	1.5424987	103.5893716	1287
25	1.5354815	103.5815447	1.5332561	103.5775431	509
26	1.5386339	103.5815447	1.5358403	103.5769669	596
27	1.5417290	103.5815447	1.5432333	103.5769435	538
28	1.4855595	103.5846387	1.4649903	103.5846592	2286
29	1.5417290	103.5846387	1.5335990	103.5639818	2466
30	1.5417290	103.5877900	1.5440528	103.5947821	818
31	1.5448241	103.5877900	1.5427280	103.5722776	1739
32	1.5448241	103.5939779	1.5371582	103.5751559	2258
33	1.5479765	103.5970719	1.5521852	103.5801907	1933
34	1.5479765	103.6001659	1.5620113	103.5969740	1599
35	1.5479765	103.6032598	1.5389201	103.5825370	2512
36	1.5573191	103.6063538	1.5558938	103.6006152	657
37	1.5510716	103.6094478	1.5651172	103.6194986	1919
38	1.5573191	103.6094478	1.5562910	103.6032236	701
39	1.5510716	103.6125418	1.5438855	103.5981747	1785
40	1.5542240	103.6125418	1.5461241	103.6027938	1408
41	1.5573191	103.6125418	1.5559136	103.6080040	528
42	1.5510716	103.6156357	1.5561084	103.6221420	914
43	1.5542240	103.6187297	1.5435775	103.6052821	1905
44	1.5542240	103.6218237	1.5501585	103.6135015	1029
45	1.5573191	103.6218237	1.5548126	103.6017478	2247
46	1.5573191	103.6249749	1.5473069	103.6003614	2952
47	1.5573191	103.6280689	1.5320676	103.5859032	5460
48	1.5604716	103.6280689	1.5806226	103.6293536	2244
49	1.5573191	103.6311629	1.5570808	103.6222517	990
50	1.5604716	103.6311629	1.5590645	103.6832645	5789
51	1.5542240	103.6342569	1.5539429	103.6209361	1480
52	1.5573191	103.6373508	1.5372266	103.6319107	2313
53	1.5448241	103.6404448	1.5236385	103.6418428	2359
54	1.5479765	103.6404448	1.4799744	103.6419449	7558
55	1.5510716	103.6404448	1.5418758	103.6403252	1022
56	1.4731222	103.6435388	1.4776887	103.6422290	528
57	1.5354815	103.6435388	1.5283755	103.6434542	790
58	1.5417290	103.6435388	1.5358823	103.6438353	651
59	1.5448241	103.6435388	1.5494699	103.6433300	517
60	1.5479765	103.6435388	1.5802535	103.6433804	3587
61	1.5542240	103.6435388	1.5542965	103.6278882	1738
Quadrant 4					

(*continued on next page*)

(*continued*)

Quadrant 4					
Input point number presented in Fig. 15 (d)	Input points in Fig. 15 (d)		ANN output points in Fig. 17		Distances between input points and ANN output points (m)
	Latitude	Longitude	Latitude	Longitude	
Input point number presented in Fig. 15 (d)	Input points in Fig. 15 (d)		ANN output points in Fig. 17		Distances between input points and ANN output points (m)
	Latitude	Longitude	Latitude	Longitude	
1	1.5947474	103.5536990	1.5935466	103.5582690	525
2	1.5978999	103.5536990	1.5975394	103.5583380	517
3	1.6009951	103.5536990	1.5972906	103.5624257	1053
4	1.6041476	103.5536990	1.5965366	103.5650552	1519
5	1.6072428	103.5536990	1.5894256	103.5648089	2333
6	1.6103380	103.5536990	1.5919260	103.5912255	4643
7	1.6134905	103.5536990	1.5998429	103.5773964	3038
8	1.6165857	103.5536990	1.6104259	103.5705859	1997
9	1.6197382	103.5536990	1.6116709	103.5687664	1899
10	1.6228334	103.5536990	1.6171267	103.5655236	1458
11	1.6259287	103.5536990	1.6249201	103.5609759	816
12	1.6290812	103.5536990	1.6285879	103.5588781	578
13	1.5947474	103.5567930	1.5926787	103.5621802	641
14	1.5978999	103.5567930	1.5964782	103.5620509	605
15	1.6009951	103.5567930	1.5962948	103.5653352	1083
16	1.6041476	103.5567930	1.5906505	103.5711722	2191
17	1.6072428	103.5567930	1.5929869	103.5726704	2371
18	1.6103380	103.5567930	1.6010766	103.5807521	2853
19	1.6134905	103.5567930	1.6078373	103.5736820	1978
20	1.6165857	103.5567930	1.6093714	103.5706599	1736
21	1.6197382	103.5567930	1.6145714	103.5679156	1362
22	1.6228334	103.5567930	1.6217512	103.5640906	819
23	1.6259287	103.5567930	1.6254234	103.5621596	599
24	1.5947474	103.5598869	1.5917937	103.5660275	757
25	1.5978999	103.5598869	1.5956591	103.5653531	656
26	1.6009951	103.5598869	1.5954455	103.5670558	1007
27	1.6041476	103.5598869	1.5828484	103.5675319	2515
28	1.6072428	103.5598869	1.5936575	103.5883360	3502
29	1.6103380	103.5598869	1.6046905	103.5770444	2006
30	1.6134905	103.5598869	1.6069085	103.5730400	1634
31	1.6165857	103.5598869	1.6121343	103.5699767	1225
32	1.6197382	103.5598869	1.6190227	103.5670815	803
33	1.6228334	103.5598869	1.6223998	103.5653950	614
34	1.6259287	103.5598869	1.6244889	103.5650815	599
35	1.5947474	103.5629809	1.5910193	103.5697465	858
36	1.5978999	103.5629809	1.5911691	103.5730693	1347
37	1.6009951	103.5629809	1.5950222	103.5664698	769
38	1.6041476	103.5629809	1.5927171	103.5831102	2571
39	1.6072428	103.5629809	1.5984325	103.5809014	2218
40	1.6103380	103.5629809	1.6076394	103.5752866	1399
41	1.6134905	103.5629809	1.6097269	103.5722613	1112
42	1.6165857	103.5629809	1.6140530	103.5703334	864
43	1.6197382	103.5629809	1.6197104	103.5684281	605
44	1.5978999	103.5660749	1.5913323	103.5735727	1107
45	1.6009951	103.5660749	1.5715175	103.5727316	3358
46	1.6041476	103.5660749	1.5952233	103.5864175	2468
47	1.6072428	103.5660749	1.6047375	103.5782542	1381
48	1.6103380	103.5660749	1.6074934	103.5740936	945
49	1.6134905	103.5660749	1.6116503	103.5725266	745
50	1.6165857	103.5660749	1.6151831	103.5716820	642
51	1.6197382	103.5660749	1.6187243	103.5705085	505
52	1.5947474	103.5691689	1.5903839	103.5745972	774
53	1.6009951	103.5691689	1.5960398	103.5880848	2172
54	1.6041476	103.5691689	1.5996901	103.5807041	1374
55	1.6072428	103.5691689	1.6066862	103.5774138	918
56	1.6103380	103.5691689	1.6102535	103.5754869	702
57	1.6134905	103.5691689	1.6127264	103.5737290	514
58	1.6009951	103.5722628	1.5983076	103.5867487	1637
59	1.6041476	103.5722628	1.6030723	103.5783798	690
60	1.5823095	103.5753568	1.5836240	103.5708829	518
61	1.5947474	103.5753568	1.5938002	103.5684357	776
62	1.5978999	103.5753568	1.5934280	103.5949739	2235
63	1.6009951	103.5753568	1.6007238	103.5808227	608
64	1.5823095	103.5784508	1.5837138	103.5736956	551
65	1.5978999	103.5784508	1.5979780	103.5844819	670
66	1.5823095	103.5815447	1.5837347	103.5768114	549
67	1.5854046	103.5815447	1.5874071	103.5774273	509
68	1.5916523	103.5815447	1.5932008	103.5689315	1412
69	1.5947474	103.5815447	1.5932108	103.5957588	1588
70	1.5978999	103.5815447	1.6005815	103.5853144	514

(*continued on next page*)

(*continued*)

Quadrant 4					
Input point number presented in Fig. 15 (d)	Input points in Fig. 15 (d)		ANN output points in Fig. 17		Distances between input points and ANN output points (m)
	Latitude	Longitude	Latitude	Longitude	
71	1.5791570	103.5846387	1.5807588	103.5795810	589
72	1.5823095	103.5846387	1.5838725	103.5800552	538
73	1.5854046	103.5846387	1.5858794	103.5801612	500
74	1.5884998	103.5846387	1.5908346	103.5770742	879
75	1.5916523	103.5846387	1.5921644	103.5702075	1604
76	1.5978999	103.5846387	1.6025364	103.5820856	588
77	1.5791570	103.5877900	1.5805933	103.5823224	628
78	1.5823095	103.5877900	1.5832594	103.5820099	651
79	1.5854046	103.5877900	1.5875742	103.5806864	825
80	1.5884998	103.5877900	1.5917449	103.5701147	1996
81	1.5947474	103.5877900	1.6009535	103.5834393	842
82	1.5978999	103.5877900	1.6017550	103.5849902	529
83	1.5791570	103.5908840	1.5806160	103.5859033	577
84	1.5823095	103.5908840	1.5839298	103.5835368	836
85	1.5854046	103.5908840	1.5898418	103.5779434	1520
86	1.5884998	103.5908840	1.5954730	103.5795170	1481
87	1.5916523	103.5908840	1.5992595	103.5854266	1040
88	1.5760619	103.5939779	1.5771963	103.5885574	615
89	1.5791570	103.5939779	1.5813044	103.5879056	715
90	1.5823095	103.5939779	1.5856038	103.5838822	1180
91	1.5854046	103.5939779	1.5904317	103.5676531	2977
92	1.5884998	103.5939779	1.5935911	103.5948680	574
93	1.5760619	103.5970719	1.5773894	103.5913165	656
94	1.5791570	103.5970719	1.5814988	103.5891393	919
95	1.5823095	103.5970719	1.5911690	103.5793705	2199
96	1.5854046	103.5970719	1.5975056	103.5879784	1682
97	1.5916523	103.5970719	1.5962606	103.5921252	751
98	1.6009951	103.5970719	1.6000147	103.6015912	514
99	1.5760619	103.6001659	1.5774551	103.5927139	842
100	1.5791570	103.6001659	1.5833282	103.5881165	1416
101	1.5823095	103.6001659	1.5813764	103.5698205	3372
102	1.5854046	103.6001659	1.5966318	103.5897630	1700
103	1.5884998	103.6001659	1.5951891	103.5928462	1102
104	1.5947474	103.6001659	1.5936153	103.6046840	517
105	1.6509198	103.6001659	1.6463654	103.6040341	664
106	1.5760619	103.6032598	1.5785706	103.5929297	1181
107	1.5791570	103.6032598	1.5915543	103.5809214	2838
108	1.5823095	103.6032598	1.5956845	103.5908026	2031
109	1.6446720	103.6032598	1.6399231	103.6053002	574
110	1.6477673	103.6032598	1.6400442	103.6060931	914
111	1.6509198	103.6032598	1.6410980	103.6083513	1229
112	1.5760619	103.6063538	1.5804923	103.5927072	1594
113	1.5791570	103.6063538	1.5792186	103.5999010	717
114	1.5823095	103.6063538	1.5872280	103.6022998	708
115	1.5854046	103.6063538	1.5892572	103.6012606	709
116	1.6415768	103.6063538	1.6368962	103.6091481	606
117	1.6446720	103.6063538	1.6356951	103.6094421	1055
118	1.6477673	103.6063538	1.6369256	103.6117251	1344
119	1.6509198	103.6063538	1.6361260	103.6133065	1816
120	1.5760619	103.6094478	1.5876218	103.5839482	3110
121	1.5791570	103.6094478	1.5932368	103.5948873	2250
122	1.5884998	103.6094478	1.5869935	103.6137029	501
123	1.6353290	103.6094478	1.6305637	103.6108141	551
124	1.6384242	103.6094478	1.6312174	103.6119152	846
125	1.6415768	103.6094478	1.6336517	103.6139718	1014
126	1.6446720	103.6094478	1.6332589	103.6156639	1444
127	1.6477673	103.6094478	1.6286046	103.6168310	2282
128	1.6509198	103.6094478	1.6284178	103.6201281	2768
129	1.5729094	103.6125418	1.5768948	103.5988639	1583
130	1.5760619	103.6125418	1.5955000	103.5652683	5678
131	1.5791570	103.6125418	1.5877959	103.6011012	1593
132	1.6321764	103.6125418	1.6268565	103.6146542	636
133	1.6353290	103.6125418	1.6303099	103.6165624	714
134	1.6384242	103.6125418	1.6250738	103.6185318	1626
135	1.6415768	103.6125418	1.6169773	103.6228127	2962
136	1.6446720	103.6125418	1.6137367	103.6226642	3617
137	1.6477673	103.6125418	1.6359223	103.6133216	1319
138	1.5729094	103.6156357	1.5874927	103.5856286	3706
139	1.6290812	103.6156357	1.6201810	103.6206391	1134
140	1.6321764	103.6156357	1.6230725	103.6221933	1247
141	1.6353290	103.6156357	1.6271630	103.6166473	914
142	1.6477673	103.6156357	1.6342221	103.6215730	1643
143	1.6509198	103.6156357	1.6402618	103.6206830	1310

(*continued on next page*)

(*continued*)

Quadrant 4					
Input point number presented in Fig. 15 (d)	Input points in Fig. 15 (d)		ANN output points in Fig. 17		Distances between input points and ANN output points (m)
	Latitude	Longitude	Latitude	Longitude	
144	1.5666618	103.6187297	1.5633472	103.6267952	969
145	1.5698143	103.6187297	1.5759208	103.6038323	1788
146	1.5729094	103.6187297	1.6031625	103.5781078	5627
147	1.6259287	103.6187297	1.6355843	103.6124156	1282
148	1.6321764	103.6187297	1.6415217	103.6149402	1121
149	1.6415768	103.6187297	1.6358066	103.6202234	662
150	1.6477673	103.6187297	1.6434927	103.6210320	539
151	1.6509198	103.6187297	1.6461743	103.6210983	589
152	1.5635667	103.6218237	1.5694385	103.6206280	666
153	1.5666618	103.6218237	1.5619352	103.6328077	1328
154	1.5698143	103.6218237	1.5889049	103.5858499	4524
155	1.6103380	103.6218237	1.6182814	103.6209071	889
156	1.6134905	103.6218237	1.6286367	103.6174149	1753
157	1.6197382	103.6218237	1.6102454	103.6251382	1117
158	1.6228334	103.6218237	1.6307882	103.6206696	893
159	1.6259287	103.6218237	1.6328082	103.6208362	772
160	1.6384242	103.6218237	1.6340916	103.6237078	525
161	1.5604716	103.6249749	1.5595770	103.6125809	1380
162	1.5635667	103.6249749	1.5709293	103.6246607	819
163	1.5698143	103.6249749	1.5818268	103.6091738	2205
164	1.5791570	103.6249749	1.5829033	103.6220677	527
165	1.5823095	103.6249749	1.5868323	103.6235125	528
166	1.5978999	103.6249749	1.6027373	103.6233337	568
167	1.6009951	103.6249749	1.6292144	103.6155885	3305
168	1.6041476	103.6249749	1.5845461	103.6249489	2178
169	1.6103380	103.6249749	1.6282886	103.6204499	2057
170	1.6134905	103.6249749	1.6268234	103.6215320	1530
171	1.5635667	103.6280689	1.5700949	103.6322381	861
172	1.5666618	103.6280689	1.5892163	103.6088943	3289
173	1.5729094	103.6280689	1.5794127	103.6207934	1084
174	1.5760619	103.6280689	1.5840254	103.6239886	994
175	1.5854046	103.6280689	1.5804628	103.6255858	615
176	1.5884998	103.6280689	1.6088942	103.6192949	2467
177	1.5916523	103.6280689	1.6321738	103.6122758	4832
178	1.5947474	103.6280689	1.5847280	103.6273678	1116
179	1.5978999	103.6280689	1.6236479	103.6188237	3040
180	1.6009951	103.6280689	1.6133380	103.6235074	1462
181	1.6041476	103.6280689	1.6142575	103.6243631	1196
182	1.5666618	103.6311629	1.5709696	103.6255544	786
183	1.5698143	103.6311629	1.5837606	103.6186288	2083
184	1.5729094	103.6311629	1.5777686	103.6268719	720
185	1.5760619	103.6311629	1.5783460	103.6265949	567
186	1.5791570	103.6311629	1.6176550	103.6133999	4711
187	1.5823095	103.6311629	1.6043328	103.6167375	2925
188	1.5854046	103.6311629	1.6264924	103.6178733	4798
189	1.5884998	103.6311629	1.6129550	103.6244001	2819
190	1.5916523	103.6311629	1.5958646	103.6294078	507
191	1.5604716	103.6342569	1.6784941	103.6346988	13115
192	1.5666618	103.6342569	1.6226509	103.5985405	7379
193	1.5698143	103.6342569	1.5879088	103.6200010	2559
194	1.5729094	103.6342569	1.6014789	103.6253434	3325
195	1.5760619	103.6342569	1.6107430	103.6294499	3891
196	1.5823095	103.6342569	1.5764354	103.6352212	661
197	1.5854046	103.6342569	1.5798082	103.6364878	669
198	1.5884998	103.6342569	1.5827293	103.6353849	653
199	1.5635667	103.6373508	1.5402894	103.6363033	2589
200	1.5698143	103.6373508	1.5909084	103.6784553	5132
201	1.5729094	103.6373508	1.5763766	103.6480143	1246
202	1.5666618	103.6404448	1.5618292	103.6401840	538
203	1.5698143	103.6404448	1.5556311	103.6375718	1608
204	1.5729094	103.6404448	1.5821208	103.6485148	1361
205	1.5791570	103.6404448	1.5795036	103.6460162	620
206	1.5666618	103.6435388	1.5665936	103.5793988	7125
207	1.5729094	103.6435388	1.5821240	103.6844289	4656
208	1.5760619	103.6435388	1.5763131	103.6182041	2814

References

Asfur, M., Price, C., Silverman, J., Wishkerman, A., 2020. Why is lightning more intense over the oceans? J. Atmos. Sol. Terr. Phys. 202, 105259. https://doi.org/10.1016/j.jastp.2020.105259.

Bala, K., Choubey, D.K., Paul, S., 2017. Soft computing and data mining techniques for thunderstorms and lightning prediction: a survey, 2017 International conference of electronics. Comm. Aerosp. Technol. (ICECA) 42–46.

Bates, B.C., Dowdy, A.J., Chandler, R.E., 2018. Lightning prediction for Australia using multivariate analyses of large-scale Atmospheric variables. J Appl Meteorol Clim 57 (3), 525–534. https://doi.org/10.1175/jamc-d-17-0214.1.

Bent, R.B., Casper, P.W., Scheffler, T.H., Leep, R., 1983. A unique time of arrival technique for accurately locating lightning over large areas. Preprints 505–511.
Chen, M., Lu, T., Du, Y., 2015. An improved wave impedance approach for locating close lightning stroke from single station observation and its validation. J. Atmos. Sol. Terr. Phys. 122, 1–8. https://doi.org/10.1016/j.jastp.2014.11.001.
Choudhury, S., Mitra, S., Chakraborty, H., 2004. A Connectionist Approach to Thunderstorm Forecasting, pp. 330–334.
Cummins, K.L., Murphy, M.J., 2009. An overview of lightning locating systems: history, techniques, and data uses, with an in-depth look at the US NLDN. Ieee T Electromagn C 51 (3), 499–518. https://doi.org/10.1109/Temc.2009.2023450.
Cummins, K.L., Murphy, M.J., Bardo, E.A., Hiscox, W.L., Pyle, R.B., Pifer, A.E., 1998. A combined TOA/MDF technology upgrade of the US national lightning detection network. J. Geophys. Res. Atmos. 103 (D8), 9035–9044.
Cummins, K.L., Murphy, M., Demetriades, N., Pifer, B., Pessi, A., Businger, S., 2008. Modeling and Calibration of Vaisala's Operational Long Range Lightning Detection Network.
Ekonomou, L., Liatsis, P., Gonos, I.F., Stathopulos, I.A., 2006. Artificial neural network-based software tool for calculating the lightning performance of high-voltage transmission lines. Iee P-Sci Meas Tech 153 (5), 188–193.
Ekonomou, L., Gonos, I.F., Iracleous, D.P., Stathopulos, I.A., 2007. Application of artificial neural network methods for the lightning performance evaluation of Hellenic high voltage transmission lines. Elec. Power Syst. Res. 77 (1), 55–63.
Gardner, M.W., Dorling, S.R., 1998. Artificial neural networks (the multilayer perceptron)—a review of applications in the atmospheric sciences. Atmos. Environ. 32 (14–15), 2627–2636. https://doi.org/10.1016/S1352-2310(97)00447-0.
Gulyás, A., Németh, B., Szonda, S., Berta, I., 2006. Application of Preventive Measures in Lightning Protection, 8-1.
Jiang, R., Qie, X., Wu, Z., Wang, D., Liu, M., Lu, G., Liu, D., 2014. Characteristics of upward lightning from a 325-m-tall meteorology tower. Atmos. Res. 149, 111–119. https://doi.org/10.1016/j.atmosres.2014.06.007.
Jiang, R., Lyu, W., Wu, B., Qi, Q., Ma, Y., Su, Z., Wu, S., Xie, Z., Tan, Y., 2020. Simulation of cloud-to-ground lightning strikes to structures based on an improved stochastic lightning model. J. Atmos. Sol. Terr. Phys. 203, 105274. https://doi.org/10.1016/j.jastp.2020.105274.
Johari, D., Rahman, T.K.A., Musirin, I., Aminudin, N., 2010. Application of meta-evolutionary programming in ANN-based lightning prediction system. Int Rev Electr Eng-I 5 (4), 1824–1832.
Kadir, M., Misbah, N.R., Gomes, C., Jasni, J., Wan Ahmad, W.F., Hassan, M.K., 2012. Recent Statistics on Lightning Fatalities in Malaysia, pp. 1–5.
Keogh, S.J., Hibbett, E., Nash, J., Eyre, J., 2006. The Met Office Arrival Time Difference (ATD) system for thunderstorm detection and lightning location. Met Met Office Forecast. Res. Tech. RepOffice Forecasting Research Tech. Rep 488, 22.
Koshak, W.J., Solakiewicz, R.J., 2001. TOA lightning location retrieval on spherical and oblate spheroidal Earth geometries. J. Atmos. Ocean. Technol. 18 (2), 187–199, 1520-0426.
Maier, M.W., Binford, R.C., Byerley, L.G., Krider, E.P., Pifer, A.E., Uman, M.A., 1983. Locating Cloud-To-Ground Lightning with Wideband Magnetic Direction Finders, pp. 497–504.
Maqsood, I., Khan, M.R., Huang, G.H., Abdalla, R., 2005. Application of soft computing models to hourly weather analysis in southern Saskatchewan, Canada. Eng. Appl. Artif. Intell. 18 (1), 115–125, 0952-1976.
Marquardt, D.W., 1963. An algorithm for least-squares estimation of nonlinear parameters. J. Soc. Ind. Appl. Math. 11 (2), 431–441, 0368-4245.
McCann, D.W., 1992. A neural network short-term forecast of significant thunderstorms. Weather Forecast. 7 (3), 525–534. https://doi.org/10.1175/1520-0434(1992)007.
Mehranzamir, K., 2015. Lightning Ground Flash Locating System Based on Combined Sensing Method Using Artificial Neural Network and Particle Swarm Optimization (Doctoral dissertation, Universiti Teknologi Malaysia). Univ. Teknol. Malaysia.
Mehranzamir, K., Davarpanah, M., Abdul-Malek, Z., Afrouzi, H.N., 2018. Discriminating cloud to ground lightning flashes based on wavelet analysis of electric field signals. J. Atmos. Sol. Terr. Phys. 181, 127–140. https://doi.org/10.1016/j.jastp.2018.11.005.
Orville, R.E., 1994. Cloud-to-ground lightning flash characteristics in the contiguous United States: 1989–1991. J. Geophys. Res.: Atmosphere 99 (D5), 12156–12202, 10833-10841.
Rakov, V.A., 2016. Electromagnetic Methods of Lightning Location, Fundamentals of Lightning. Cambridge University Press, pp. 161–177. https://doi.org/10.1017/CBO9781139680370.009.
Reynaldi, A., Lukas, S., Margaretha, H., 2012. Backpropagation and Levenberg-Marquardt Algorithm for Training Finite Element Neural Network, pp. 89–94.
Salimi, Behnam, Abdul-Malek, Zulkurnain, Mehranzamir, Kamyar, Mashak, Saeed Vahabi, Afrouzi, H.N., 2013. Localised single-station lightning detection by using TOA method. J. Teknol. 64 (4), 73–77. https://doi.org/10.11113/jt.v64.2105.
Sathya, R., Abraham, A., 2013. Comparison of supervised and unsupervised learning algorithms for pattern classification. Int. J. Adv. Res. Artif. Intell. 2 (2), 34–38.
Siingh, D., Singh, R.P., Kumar, S., Dharmaraj, T., Singh, A.K., Singh, A.K., Patil, M.N., Singh, S., 2015. Lightning and middle atmospheric discharges in the atmosphere. J. Atmos. Sol. Terr. Phys. 134, 78–101. https://doi.org/10.1016/j.jastp.2015.10.001.
Silva, I.N.D., Souza, A.N.D., Bordon, M.E., 1999. Evaluation and identification of lightning models by artificial neural networks, Neural Networks, 1999. IJCNN '99. Int. Joint Conf. 3816, 3816–3820. https://doi.org/10.1109/IJCNN.1999.830762.
Singh, A.K., Siingh, D., Singh, R.P., 2011. Impact of galactic cosmic rays on Earth's atmosphere and human health. Atmos. Environ. 45 (23), 3806–3818. https://doi.org/10.1016/j.atmosenv.2011.04.027.
Sivanandam, S.N., Deepa, S.N., 2006. Introduction to Neural Networks Using Matlab 6.0. Tata McGraw-Hill Education.
Sun, Z., Qie, X., Liu, M., Cao, D., Wang, D., 2013. Lightning VHF radiation location system based on short-baseline TDOA technique — validation in rocket-triggered lightning. Atmos. Res. 129–130, 58–66. https://doi.org/10.1016/j.atmosres.2012.11.010.
Underwood, S.J., 2006. Cloud-to-ground lightning flash parameters associated with heavy rainfall alarms in the Denver, Colorado, Urban Drainage and Flood Control District ALERT network. Mon. Weather Rev. 134 (9), 2566–2580.
Vahabi-Mashak, S., Abdul-Malek, Z., Mehranzamir, K., Nabipour-Afrouzi, H., Salimi, B., Wooi, C.-L., 2015. Modeling of time of arrival method for lightning locating systems. Adv. Meteorol. 2015, 12. https://doi.org/10.1155/2015/870290.
Valero, S., Aparicio, J., Senabre, C., Ortiz, M., Sancho, J., Gabaldon, A., 2010. Comparative Analysis of Self Organizing Maps vs. Multilayer Perceptron Neural Networks for Short-Term Load Forecasting, pp. 1–5.
Wang, D., Wu, T., Takagi, N., 2018. Charge structure of winter thunderstorm in Japan: a review and an update. IEEJ Trans. Power and Energy 138 (5), 310–314. https://doi.org/10.1541/ieejpes.138.310.
Wood, T.G., Inan, U.S., 2003. Combined TOA/MDF Lightning Location Using Three Globally Distant Sites, 0161.
Yaniv, R., Yair, Y., Price, C., Mkrtchyan, H., Lynn, B., Reymers, A., 2017. Ground-based measurements of the vertical E-field in mountainous regions and the "Austausch" effect. Atmos. Res. 189, 127–133. https://doi.org/10.1016/j.atmosres.2017.01.018.
Yu, H., Wilamowski, B.M., 2011. Levenberg-marquardt training. Ind. Electr. Handbook 5, 12-11.